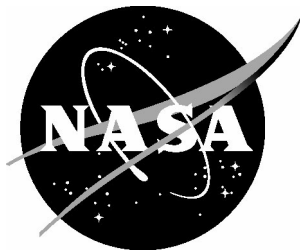
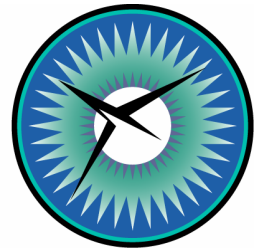


NASA/CR-2013-217959
NIA Report No. 2013-0115



NATIONAL
INSTITUTE OF
AEROSPACE



Characterizing Facesheet/Core Disbonding in Honeycomb Core Sandwich Structure

Martin Rinker

Fraunhofer-Institut für Werkstoffmechanik IWM, Halle, Germany

James G. Ratcliffe

National Institute of Aerospace, Hampton, Virginia

Daniel O. Adams

University of Utah, Salt Lake City, Utah

Ronald Krueger

National Institute of Aerospace, Hampton, Virginia

NASA STI Program . . . in Profile

Since its founding, NASA has been dedicated to the advancement of aeronautics and space science. The NASA scientific and technical information (STI) program plays a key part in helping NASA maintain this important role.

The NASA STI program operates under the auspices of the Agency Chief Information Officer. It collects, organizes, provides for archiving, and disseminates NASA's STI. The NASA STI program provides access to the NASA Aeronautics and Space Database and its public interface, the NASA Technical Report Server, thus providing one of the largest collections of aeronautical and space science STI in the world. Results are published in both non-NASA channels and by NASA in the NASA STI Report Series, which includes the following report types:

- **TECHNICAL PUBLICATION.** Reports of completed research or a major significant phase of research that present the results of NASA Programs and include extensive data or theoretical analysis. Includes compilations of significant scientific and technical data and information deemed to be of continuing reference value. NASA counterpart of peer-reviewed formal professional papers, but having less stringent limitations on manuscript length and extent of graphic presentations.
- **TECHNICAL MEMORANDUM.** Scientific and technical findings that are preliminary or of specialized interest, e.g., quick release reports, working papers, and bibliographies that contain minimal annotation. Does not contain extensive analysis.
- **CONTRACTOR REPORT.** Scientific and technical findings by NASA-sponsored contractors and grantees.

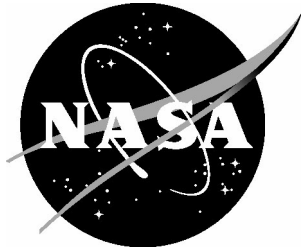
- **CONFERENCE PUBLICATION.** Collected papers from scientific and technical conferences, symposia, seminars, or other meetings sponsored or co-sponsored by NASA.
- **SPECIAL PUBLICATION.** Scientific, technical, or historical information from NASA programs, projects, and missions, often concerned with subjects having substantial public interest.
- **TECHNICAL TRANSLATION.** English-language translations of foreign scientific and technical material pertinent to NASA's mission.

Specialized services also include organizing and publishing research results, distributing specialized research announcements and feeds, providing information desk and personal search support, and enabling data exchange services.

For more information about the NASA STI program, see the following:

- Access the NASA STI program home page at <http://www.sti.nasa.gov>
- E-mail your question to help@sti.nasa.gov
- Fax your question to the NASA STI Information Desk at 443-757-5803
- Phone the NASA STI Information Desk at 443-757-5802
- Write to:
STI Information Desk
NASA Center for AeroSpace Information
7115 Standard Drive
Hanover, MD 21076-1320

NASA/CR-2013-217959
NIA Report No. 2013-0115



Characterizing Facesheet/Core Disbonding in Honeycomb Core Sandwich Structure

Martin Rinker
Fraunhofer-Institut für Werkstoffmechanik IWM, Halle, Germany

James G. Ratcliffe
National Institute of Aerospace, Hampton, Virginia

Daniel O. Adams
University of Utah, Salt Lake City, Utah

Ronald Krueger
National Institute of Aerospace, Hampton, Virginia

National Aeronautics and
Space Administration

Langley Research Center
Hampton, Virginia 23681-2199

Prepared for Langley Research Center
under Cooperative Agreement NNL09AA00A

February 2013

Trade names and trademarks are used in this report for identification only. Their usage does not constitute an official endorsement, either expressed or implied, by the National Aeronautics and Space Administration.

Available from:

NASA Center for AeroSpace Information
7115 Standard Drive
Hanover, MD 21076-1320
443-757-5802

Characterizing Facesheet/Core Disbonding in Honeycomb Core Sandwich Structure

Martin Rinker¹, James Ratcliffe², Dan Adams³, and Ronald Krueger²

Abstract

Results are presented from an experimental investigation into facesheet core disbonding in carbon fiber reinforced plastic / Nomex honeycomb sandwich structures using a Single Cantilever Beam test. Specimens with three, six and twelve-ply facesheets were tested. Specimens with different honeycomb cores consisting of four different cell sizes were also tested, in addition to specimens with three different widths.

Three different data reduction methods were employed for computing apparent fracture toughness values from the test data, namely an area method, a compliance calibration technique and a modified beam theory method. The compliance calibration and modified beam theory approaches yielded comparable apparent fracture toughness values, which were generally lower than those computed using the area method. Disbonding in the three-ply facesheet specimens took place at the facesheet/core interface and yielded the lowest apparent fracture toughness values. Disbonding in the six and twelve-ply facesheet specimens took place within the core, near to the facesheet/core interface. Specimen width was not found to have a significant effect on apparent fracture toughness. The amount of scatter in the apparent fracture toughness data was found to increase with honeycomb core cell size.

1 Introduction

Sandwich structure can offer superior mechanical performance over traditional structural configurations. However, this type of structure can exhibit several different failure modes, the occurrence of which is dependent largely on the configuration of the sandwich structure (constituent materials) and loading scenario [1]. One such failure mode, facesheet/core disbonding, can pose a threat to the structural integrity of a component comprised of sandwich structure. Consequently, manufacturers typically gauge the quality of the facesheet/core bond using a climbing drum peel (CDP) test [2]. Although this yields a qualitative assessment of the bond, use of data from this test for damage tolerance design purposes is limited. Although, recent work suggests that it may be possible to estimate the critical strain energy release rate associated with facesheet/core peel in thin facesheet sandwich panels using the CDP test [3].

As is the case with mode I delamination in monolithic laminates, the most critical disbonding process in sandwich structure is likely to be mode I dominated, corresponding to loading scenarios where the facesheet is peeled from the core. Subsequently, the literature is focused on test methods designed to measure the critical strain energy release rate associated with facesheet/core peel. Thus, numerous alternative test methods have arisen from the need for a quantitative assessment of the facesheet/core bond [3-26]. These test methods largely follow a

¹ Fraunhofer-Institut für Werkstoffmechanik IWM, Halle, Germany

² National Institute of Aerospace, Hampton, Virginia, USA

³ University of Utah, Salt Lake City, Utah, USA

common approach, whereby facesheet/core disbonding is characterized through the measurement of the corresponding critical strain energy release rate (referred to in this paper as apparent fracture toughness).

Two general classes of facesheet/core peel test specimens have been developed. The overall specimen configuration used in both classes is similar, involving a sandwich beam containing a disbond running partially along one of the facesheet/core interfaces. The first class of specimens is based on a single cantilever beam (SCB) configuration (Figure 1a), where force is applied to the disbanded facesheet, while the underside of the specimen is secured to a rigid base and prevented from rotation. The second class of specimens is based on a double cantilever beam (DCB) design, where equal and opposite forces are applied to the specimen, either side of the disbond, as illustrated in Figure 1b.

In a recent study, the suitability of several of the aforementioned test methods for measuring apparent fracture toughness associated with facesheet/core peel was evaluated [4]. A SCB-type specimen, with a configuration identical to that shown in Figure 1a, was identified as the most appropriate test. This determination was based on the following: (1) the test involves a simple loading fixture, (2) disbond front loading conditions were found to be independent of disbond length, (3) disbonding was found to take place along or near to the facesheet/core interface, rather than kinking into the core, (4) the data reduction method utilized for computing apparent fracture toughness involves a straightforward compliance calibration procedure.

Partly in response to these findings, a recent effort was initiated to develop a standardized test method for measuring the apparent fracture toughness of sandwich structure [27-29]. This involved the development of a procedure for determining the SCB specimen dimensions (specimen length, facesheet thickness, initial disbond length). This sizing method helps ensure that a specimen behaves in a suitable manner during a test. That is, for the purposes of data reduction, specimen response should be linear elastic and the specimen exhibits a specific disbond length/compliance relationship (compliance solution) [27].

A consequence of this sizing approach is that the facesheet thickness specified for the SCB specimen may differ from that of the in-service sandwich configuration. As the disbond in an SCB specimen is essentially an interface crack, the opening and shear tractions local to the disbond front are coupled, and as is the case of this specimen, a mixed mode-I/II loading condition arises along the disbond front. Assuming that apparent fracture toughness is a significant function of mode mix (as demonstrated in recent articles [25-26]), it is therefore possible that the measured apparent fracture toughness could differ from the toughness of the in-service sandwich panel if specimen facesheet thickness differs sufficiently from that in the actual sandwich configuration.

Furthermore, the SCB sizing method does not offer a means for establishing specimen width. In general, an upper limit is prescribed to the width of such specimens in order to preserve a plane strain loading condition (to help ensure specimen response is in-keeping with assumptions made in the data reduction method) and a lower limit is prescribed to ensure edge effects do not become dominant. However, added complications arise in the case of sandwich construction with honeycomb core materials. First, a minimum number of cells are required across the specimen width in order to establish an adequate representation of the honeycomb structure. Second, in the case of Nomex honeycomb cores that are based on Nomex paper impregnated in phenolic resin, core density is achieved through a variation in relative proportions of paper and resin. Consequently, fracture toughness of such honeycombs may not change in direct proportion with honeycomb density [30]. Additionally, the method involved in measuring

apparent fracture toughness operates on the assumption that smearing this measurement for a highly discontinuous structure such as honeycomb is valid.

The issues raised above concerning facesheet thickness, specimen width, and honeycomb cell size are being addressed as part of an on-going exercise geared towards standardizing the SCB test. A part of this effort is described in this technical report, where the main objectives of the current work were to investigate the effect of these parameters on the apparent fracture toughness of honeycomb-based sandwich structure measured using the SCB test. To this end, fracture toughness of several sandwich constructions based on Nomex^{®4} honeycomb core were measured using the SCB test. Specimens with three different apparent facesheet thicknesses, four cell sizes and three widths were tested. The apparent fracture toughness measured from SCB tests on each sandwich configuration are reported and discussed later in this report. Further recommendations for future research are also discussed.

2 Experimental Procedure

2.1 Materials and Specimen Manufacture

The investigated sandwich structures consisted of Nomex[®] HRH-10 honeycomb core materials manufactured by Hexcel Corporation [31]. Four honeycombs with 0.125mm, 0.188mm, 0.250mm, and 0.375mm cell sizes were utilized in the current study. The nominal density and thickness of all four variations of core was 48kg/m³ and 12.7mm, respectively. The facesheets consisted of a M30SC carbon/epoxy unidirectional prepreg tape also manufactured by Hexcel Corporation [32]. Three facesheets with different thicknesses were used. The stacking sequences of the three facesheets was [0/90/0], [0/90/0]_s and [0/90/0]_{2s}, respectively, with a nominal cured ply thickness of 0.167mm. The main reason for using cross ply facesheets was to reduce manufacturing complexity.

The sandwich panels from which SCB specimens were cut were manufactured at the University of Utah in two stages. First, the carbon/epoxy tape plies were cut into 300mm-square sheets and laid up to create the three different facesheet configurations. Each plate was cured in a hot press using a cure cycle recommended by the composite material manufacturer [32]. The second stage of the sandwich panel preparation involved bonding the pre-cured facesheets onto 300mm-square plates of honeycomb core. A FM300-1 film adhesive [33] was used to adhere the facesheets to the core material. A 76mm-wide strip of 13mm-thick polytetrafluoroethylene (PTFE) film was positioned between the core and film adhesive along one side of the sandwich plate. This served to create the artificial disbond of the SCB specimens. The resulting sandwich was vacuum bagged and cured by ramping the plate from room temperature to 177°C in a 30-minute period. The plate was held at this temperature for an additional hour at which point the film adhesive material was fully cured.

SCB specimens were cut from each cured sandwich plate, resulting in the general configuration illustrated in Figure 1a.

2.2 Test Matrix

The main purposes of this investigation were to determine the effect of facesheet thickness, honeycomb cell size and specimen width on apparent fracture toughness measured using the

⁴ Nomex[®] is a registered trademark of E.I DuPont de Nemours, Wilmington, DE, USA

SCB test. To this end, a total of fifty specimens were tested, including specimens with three different facesheet thicknesses (0.48mm, 0.95mm and 1.9mm, corresponding to 3, 6, and 12 plies, respectively) and three specimen widths (25.4mm, 50.8mm and 76.2mm) in addition to honeycomb cores with four different cell sizes (0.125mm, 0.188mm, 0.25mm and 0.375mm), dimension h in Figure 2. A summary of these specimens is given in Table 1. All specimens were tested in the L direction (ribbon direction, Figure 2) of the honeycomb core. Note, there is a possibility that the findings described herein may differ had specimens been tested along the W direction of the honeycomb core.

2.3 SCB Test Procedure

The general test procedure for conducting a SCB test is analogous to that used for characterizing mode I delamination resistance in monolithic, composite laminates, as employed in ASTM International Test Method D5528-01 [34]. The overall SCB loading fixture was based on that used in a previous investigation [26]. The fully intact side of a SCB sandwich specimen was bonded to a rigid baseplate, leaving the partially disbonded side of the specimen facing upwards. A piano hinge was then bonded to the upper facesheet in the disbonded region with a two-part epoxy adhesive (Hysol 6359). The baseplate containing the bonded specimen was then attached to a rigid lower fixture that was pre-mounted into a servo-hydraulic testing machine. The load-application point was vertically offset from the SCB specimens via a 300mm-long loading rod that connected the piano hinge bonded to the specimen to the crosshead of the test machine (see Figure 1a). The end of the loading rod attached to the crosshead was connected using a pinned configuration, thus preventing development of a moment arm in the rod. The purpose of offsetting the load application point is to ensure that loading remains essentially vertical during a test, thus preventing the accumulation of shear deformation in the core, which could introduce an unwanted mode II component of loading along the disbond front. A picture of the actual SCB test fixture with a 25.4mm-wide specimen is shown in Figure 3.

All specimens were loaded under displacement control at a quasi-static displacement rate of 0.5mm per minute in the direction indicated in Figure 1a. The loading was continued until a disbond growth increment of approximately 10mm had been observed, after which point specimens were completely unloaded. This loading cycle was repeated an additional five times, resulting in six individual disbond growth increments of approximately 10mm.

Applied load, P , and corresponding load-point displacement values, δ , were recorded continuously during each loading cycle as illustrated in Figure 4a. During all tests, load-point displacement was inferred from the machine crosshead displacement. This method of monitoring load-point displacement was found to be valid on the basis that system compliance was negligible (less than 1%) compared to specimen compliance. This was determined by loading a steel bar of known stiffness and measuring the resulting system compliance.

Digital cameras equipped with macroscopic lenses were positioned along both edges of a specimen, as shown in Figure 3. The cameras were used to record disbond front position viewed from both specimen edges at various stages of disbond growth during each loading cycle. The cameras were also linked with the data acquisition system used to collect applied load and load point-displacement data, such that values of load and displacement were recorded at the moment each picture was taken. Once a test was completed, specimens were removed from the baseplate, which was then prepared for the next test.

2.4 Data Reduction Methods

Three data reduction methods were employed for computing apparent fracture toughness from the SCB test data, namely an area method (AM), a modified beam theory method (MBT) and a compliance calibration (CC) procedure. All of the methods rely on use of linear elastic fracture mechanics.

The area method defines the apparent fracture toughness, G_c^{AM} , as:

$$G_c^{AM} = \frac{dU}{dA} \quad (1)$$

where dU is the energy dissipated (illustrated by shaded region in Figure 4a) during the creation of a disbond of area, dA (where $dA = b(a_1 - a_2)$ as illustrated in Figure 4a, where b is the specimen width).

In the case of the compliance calibration and modified beam theory procedures, the following expression for G_c is used [35]:

$$G_c = \frac{P_c^2}{2b} \frac{dC}{da} \quad (2)$$

where P_c is the force at the onset of disbond growth, b is the specimen width, and C and a are specimen compliance and disbond length, respectively.

The modified beam theory method utilizes a previously developed analytical compliance solution for the SCB specimen compliance, which is based on a beam-on-elastic foundation model and expressed as [22]:

$$C_{SCB}^{MBT} = \frac{\delta}{P} = \frac{4\lambda}{k} \left[\frac{\lambda^3 a^3}{3} + \lambda^2 a^2 F_1 + \lambda a F_2 + \frac{3ak}{10\lambda G_{xz,f} t_f b} + \frac{F_3}{2} \right] \quad (3)$$

The parameters t_f , b , and $G_{xz,f}$ are the facesheet thickness, SCB specimen width, and facesheet transverse shear modulus, respectively (subscripts relate to coordinate system in Figure 1a). The compliance coefficients, F_1 , F_2 , and F_3 are hyperbolic functions, which are described in Refs. 22 and 36. The parameter, k , is the elastic foundation modulus, and is related to the thickness-direction modulus of the core material as follows [36]:

$$k = \frac{E_c b}{t_c} \quad (4)$$

where the parameters t_c and E_c are the thickness and thickness-direction modulus of the core, respectively.

The parameter, λ , is effectively the ratio of the stiffness of the elastic foundation to the bending stiffness of the beam, and is given by [22]:

$$\lambda = \left[\frac{3k}{E_f t_f^3 b} \right]^{\frac{1}{4}} = \left[\frac{3E_c}{t_c t_f^3 E_f} \right]^{\frac{1}{4}} \quad (5)$$

where the parameter, E_f , is the flexural modulus of the facesheet.

A recent study that investigated a method for sizing SCB specimens found that the compliance solution in Eq. 3 reduces to the following form when certain in-plane specimen dimensions are kept within specific limits [28]:

$$C_{SCB}^{MBT} \approx m_1 \left(a + \frac{1}{\lambda} \right)^3 \quad (6)$$

where the parameter, m_1 , is expressed as [28]:

$$m_1 = \frac{4}{E_f b t_f^3} \quad (7)$$

Two main limits ensure that the SCB specimen compliance adopts the simplified form of Eq. 6. The first limit requires the intact portion of the SCB specimen (dimension L_b in Figure 1a) to remain larger than a minimum value (in the case of the SCB specimen, $L_b > 2.7/\lambda$). This ensures that the hyperbolic functions in Eq. 2 remain at unity. The second limit requires the initial disbond length to be kept above a minimum value to ensure that deformation of the disbanded facesheet is dominated by bending (further details of these limits can be found in Ref. 28). The SCB specimens tested in the current study were designed to satisfy these limits and thus it was assumed that the SCB specimen compliance solution adopted the form of Eq. 6.

The parameters, m_1 and $1/\lambda$ are evaluated from the relationship between $C^{1/3}$ and disbond length, as illustrated in Figure 4b. Substituting Eq. 6 into Eq. 2 for the derivative, dC/da , thus gives the modified beam theory-based expression for apparent fracture toughness, G_C^{MBT} ,

$$G_C^{MBT} = \frac{3P_C \delta}{2b \left(a + \frac{1}{\lambda} \right)} \quad (8)$$

The third data reduction method, namely compliance calibration, assumes the SCB specimen compliance adopts the following form:

$$C_{SCB}^{CC} = m_2 a^n \quad (9)$$

The parameters, m_2 and n are evaluated from the relationship between compliance and disbond length, as illustrated in Figure 4c.

Substituting Eq. 9 into Eq. 2 for the derivative, dC/da , thus gives the compliance calibration-based expression for apparent fracture toughness, G_c^{CC} ,

$$G_c^{CC} = \frac{nP_c\delta}{2ba} \quad (10)$$

3 Results/Discussion

3.1 Effect of Honeycomb Cell Size on Apparent G_c

Images of disbond propagation in SCB tests on specimens with 6-ply facesheets and 3.2, 4.8, 6.4 and 9.5mm honeycomb core cell size are shown in the left-hand side of Figures 5, 6, 7 and 8, respectively. The surfaces of the disbanded sandwich parts after these tests are shown in the right-hand side of Figures 5, 6, 7 and 8. Facesheet disbonding occurred in all specimens near the interface within the core, as indicated in Figures 5, 6, 7 and 8. Fracture surfaces of the facesheets of large cell size specimens (6.4 and 9.5 mm) also contained adhesive resin material. This indicates that the disbonding happened closer to the adhesive rich zone of the facesheet/core interface than in the small cell size specimens.

The load-displacement curves of the SCB specimens with different honeycomb cell size are shown in Figure 9, 10, 11 and 12. Load-displacement curves of specimens with the two smallest honeycomb cell sizes exhibited an initial unstable force drop (corresponding to growth onset from the PTFE insert) followed by a predominantly gradual reduction in applied force as load-point displacement increases. With increasing cell size, the load-displacement responses become more and more unstable. In the 6.4 mm cell size specimens, the disbond propagation changes from stable to partly unstable and becomes mostly unstable in the 9.5 mm cell size specimens. The observed change in the crack propagation behavior may be explained by the fact that disbonding shifted from completely propagating in the core to a location closer to the adhesive rich zone of the facesheet/core interface.

Plots of specimen compliance versus the cube root of disbond length are plotted in Figures 13, 14, 15 and 16. Linear regression analysis was performed on data from each individual specimen in order to evaluate the corresponding modified beam theory parameters, m_l and l . Plots of the log of specimen compliance versus the log of disbond length are presented in Figures 17, 18, 19 and 20. Linear regression analysis was performed on these data to determine the compliance calibration parameter, n . In all these cases (Figures 13 to 20), the coefficient of determination, R^2 , ranged between 0.9 and 0.99 indicating that the regression lines (solid lines in Figures 13 to 20) consistently fit the experimental data to a high degree. This indicates that the measured disbond lengths were reasonable regardless of the cell size of a specimen's honeycomb core.

The determined apparent fracture toughness values of all specimens with different cell size are shown in Figures 21, 22, 23 and 24. The *Area Method* (AM) (black symbols in Figures 21 to 24) resulted in one apparent fracture toughness value for each of the (mostly) six loading loops per specimen, whereas the *Compliance Calibration Method* (CC) and the *Modified Beam Theory* (MBT) (blue and red symbols, respectively, in Figures 21 to 24) gave apparent fracture toughness values for each recorded increment of disbond propagation (multiple growth increments were recorded during each of the six loading cycles). Generally, plots of apparent fracture toughness as a function of disbond length reach a plateau.

Examination of the data in Figures 21 to 24 shows that scatter of the apparent fracture toughness depends significantly on the honeycomb cell size. The standard deviation of apparent fracture toughness of the 3.2 mm cell size specimens is 7 % (AM), 7 % (CC) and 11 % (MBT). The specimens with a three times larger cell size show a standard deviation of 23 % (AM), 18 % (CC) and 19 % (MBT), an increase by a factor of 2-3. The scatter is also directly linked to the disbond propagation behavior. The standard deviation is higher for the unstable crack propagation in the adhesive rich zone of the facesheet/core interface than for the stable crack propagation completely in the core.

Figure 25 shows the average apparent fracture toughness for each cell size, which are based on apparent fracture toughness values of all specimens (error bars correspond to one standard deviation on either side of the corresponding average value of fracture toughness). In the case of the data from the area method, the first loading cycle was omitted from the average values in order to remove the influence of disbond growth onset from the PTFE insert. The PTFE insert was located directly at the adhesive resin/facesheet interface. Disbond growth in all 6-ply facesheet specimens immediately transitioned from this interface to a location within the core material, and thus growth onset from the insert was not deemed to be representative of disbond growth onset in the sandwich configurations.

The disbond tip was found to become less well defined in specimens with larger honeycomb cell sizes (indicated in the images in Figures 4-7). This introduced uncertainty into the compliance calibration and modified beam theory data reduction methods, which likely contributed to the scatter in the apparent fracture toughness values.

As shown in Figure 25, the average apparent fracture toughness shows no clear dependency on the honeycomb cell size. The difference between the smallest cell size (880 J/m² (AM), 770 J/m² (CC) and 760 J/m² (MBT)) and the largest cell size (1000 J/m² (AM), 910 J/m² (CC) and 910 J/m² (MBT)) is much smaller than the difference between 4.8 mm (780 J/m² (AM), 700 J/m² (CC) and 700 J/m² (MBT)) and 6.4 mm cell size (1190 J/m² (AM), 1010 J/m² (CC) and 1010 J/m² (MBT)). However, a discussion of the cell size effect on the apparent fracture toughness is not meaningful without knowing the cell wall material properties. Since the Nomex® paper thickness and the surrounding phenolic resin layer vary with the honeycomb density and cell size, each core configuration consists of a unique cell wall material [30].

3.2 Effect of FaceSheet Thickness and Specimen Width on Apparent G_c

Figures 8 and 26 illustrate that disbonding in the thick facesheet sandwich specimens propagated deeper in the core than in the thin facesheet specimens. Significantly more honeycomb material is evident on the disbanded facesheets in these specimens compared to the 6-ply facesheet specimens. No adhesive residue is visible on the disbanded honeycomb of the 12-ply facesheet specimens. Conversely, disbond propagation in the 3-ply facesheet specimens took place completely in the interface between facesheet and adhesive, as illustrated in Figure 27. No honeycomb material is evident on the disbanded 3-ply facesheets, and a significant amount of adhesive residue is apparent on the honeycomb side. The honeycomb pattern on the facesheets indicates that the adhesive was completely removed from the facesheets where the cell walls were bonded. The comparative disbond location in specimens with thick (Figure 26) and thin facesheets (Figure 27) clearly indicates that facesheet thickness dictates the disbond path. The coupling of shear and opening tractions local to the disbond front that arises from the mismatch in stiffness of the core and facesheet is therefore likely affecting the stress field local

to the disbond front. One possible explanation is that the shear stresses acting local to the disbond front are greater in specimens with thicker facesheets, and thus tend to drive disbonding further into the core [29].

The load-displacement curves of the 25.4 and 76.2 mm-wide SCB specimens with 6-ply facesheets are shown in Figure 28 and 29, respectively. Except for the different load levels due to the difference in specimen width, the curves are similar to those of the 50.8 mm wide specimens with 6-ply facesheets, shown in Figure 12. In all three cases, disbond propagation is mostly unstable, which is reflected in the uneven load-displacement curves. Since the disbond location in the 12-ply facesheet specimens is shifted deeper into the core away from the adhesive rich zone, the disbond propagation is mostly stable and the load-displacement curves are thus relatively smooth. Except for the different load level, the load-displacement curves of the 25.4, 50.8 and 76.2 mm wide 12-ply facesheet specimens (Figure 30, 31, and 32, respectively) are similar. The load-displacement curves of the 3-ply facesheet specimens in Figure 33 show a nonlinear loading behavior. The nonlinearity becomes visible at the second loading ramp and increases with each additional loading loop. The nonlinearity results from the very large facesheet bending, as pictured in Figure 27 (left). The large bending is a result of the relatively large deformations required for disbond propagation, resulting in significant anticlastic bending in the loaded facesheet. This effect is thought to cause the perceived stiffening as specimen loading increases as is evident in Figure 33.

Figure 34, 35 and 36 show the plots and their fitted linear equations for the apparent fracture toughness evaluation using the *Modified Beam Theory*. The log-log scale compliance calibration curves and the fitted power laws for the *Compliance Calibration Method* are shown in Figure 37, 38 and 39. As for the specimens of the previous sections, the regression curves are mostly a close fit to the experimental data. The scatter is higher only in the 3-ply facesheet specimens at longer crack lengths, which results obviously from the nonlinear loading behavior, which was computed for a given load and corresponding displacement value assuming a linear specimen response.

The apparent fracture toughness values are shown in Figure 40, 41 and 42. The average of each configuration is shown in the bar plot in Figure 43 (the first loading cycle was excluded in cases when the area method was used for data reduction). Since all specimens consist of the same honeycomb core that contains the largest cell size, the scatter is quite high for all configurations.

From Figure 43, the only exception from the *Area Method* results appear to be the values obtained from the 12-ply/25.4 mm specimens. Due to missing images during loading and unloading, only two *Area Method* apparent fracture toughness values could be evaluated instead of at least 15 per configuration. Their scatter is low but not representative. For the thin facesheet configurations, the standard deviation of fracture toughness values from the *Area Method* is 20, 23 and 12 % for the 25.4, 50.8 and 76.2 mm wide specimens, respectively. The trend of smaller scatter for wider specimens becomes apparent. Excluding the 25.4 mm wide specimens, the same trend can be seen for the 12-ply facesheet configurations. The standard deviation of fracture toughness values from the *Area Method* amounts to 20 and 13 % for the 50.8 and 76.2 mm wide specimens, respectively. No significant influence of facesheet thickness on scatter in fracture toughness values is apparent, as evidenced by the consistent level of scatter in specimens with different facesheet thicknesses. This is notable since disbond propagation was mostly unstable in specimens with thin facesheets and completely stable in the thick facesheet specimens.

The apparent fracture toughness standard deviation of the *Compliance Calibration Method* and the *Modified Beam Theory* is generally lower than of the *Area Method*. However, these values are not directly comparable because the number of apparent fracture toughness values is generally different. For the *Area Method*, always five values were available from each specimen. For the *Compliance Calibration Method* and the *Modified Beam Theory*, the number depends on the images taken during crack propagation. Especially during the stable crack propagation in the thick facesheet specimens several images were taken during each loading loop. The higher number of values is therefore probably the major reason for the lower scatter in fracture toughness observed in the thick facesheet specimens.

The apparent fracture toughness average of the *Area Method* is obviously independent of the specimen width (again excluding the 12-ply/25.4 mm results). In contrast, a significant difference is visible between the face sheet configurations. The average of all 6-ply face sheet specimens is 1030 J/m² and of all 50.8 and 76.2 mm wide 12-ply face sheet specimens 1160 J/m². The apparent fracture toughness is obviously higher when the disbond propagated deeper in the core. The apparent fracture toughness of the 3-ply specimens amounts to only 690 J/m². Here the disbond propagated entirely in the adhesive/face sheet interface. However, the nonlinear loading behavior needs to be considered for this particular configuration.

As in the last section, the *Compliance Calibration Method* and the *Modified Beam Theory* gave generally up to 10 % lower apparent fracture toughness values but the overall trends are the same as described for the *Area Method*. The only exception is the apparent dependence on the specimen width in case of the 12-ply facesheet specimens. In this configuration the apparent fracture toughness increases slightly with the specimen width.

4 Concluding Remarks

The facesheet disbonding of honeycomb core sandwich structures was investigated experimentally using the Single Cantilever Beam test. The facesheet thickness has a major influence on the disbond propagation behavior. In thin facesheet specimens, the crack propagates during SCB testing near the interface or completely out of the core in the more brittle adhesive. As a consequence, the crack propagation is mostly unstable and the apparent fracture toughness is lower compared to thick facesheet specimens.

The honeycomb cell size influences significantly the scatter of the measured apparent fracture toughness. Standard deviation increases approximately in direct proportion with cell size. The apparent fracture toughness itself varies with investigated honeycomb cell size. However, a clear trend is not obvious in the data. The Nomex[®] cell wall base material is surrounded by phenolic resin and the thickness of both components vary with the core density and the cell size. Therefore, additional information regarding the effective cell wall material and its behavior is needed to understand the influence of the cell size on the SCB apparent fracture toughness, which could form the basis of further work.

Narrow specimens exhibit lower scatter in apparent fracture toughness than wider counterparts. A clear dependency of the average apparent fracture toughness on the specimen width, however, could not be determined.

The tests were evaluated via *Area Method*, *Compliance Calibration Method* and *Modified Beam Theory*. All three methods are applicable and show qualitatively the same results. However, the *Area Method* gave about 10 % higher apparent fracture toughness values compared

to values from *Compliance Calibration Method* and *Modified Beam Theory*, results of which are nearly identical.

The tests with very thin facesheets (3 plies, 0.48 mm) showed the need for specimen sizing. The low facesheet bending stiffness in combination with long initial cracks resulted in extensive facesheet bending and thus in a nonlinear loading behavior after the first loading loop.

Acknowledgements

This work was performed at NASA Langley's Durability, Damage Tolerance and Reliability Branch. Funding from the NASA Subsonic Rotary Wing Program and Fraunhofer-Gesellschaft as part of the fellowship program is greatly appreciated. Invaluable discussions with Mr. Barry Milward of Euro Composites Inc and Dr. Ley Richardson of DuPont Inc are also greatly appreciated.

References

- [1] Allen H.G., "Analysis and Design of Structural Sandwich Panels," Pergamon Press, 1969.
- [2] American Society for Testing and Materials, "Standard Test Method for Climbing Drum Peel for Adhesives," ASTM Standard D1781-98, In: ASTM Annual Book of Standards, Vol. 15.06, ASTM, 2006.
- [3] Nettles A.T., Gregory E.D., and Jackson J.R., "Using the Climbing Drum Peel (CDP) Test to Obtain a G_{Ic} Value for Core/Face Sheet Bonds," *Journal of Composite Materials*, Vol. 41, No. 24, 2007, pp. 2863-2876.
- [4] Weaver C., "Evaluation of Mode I Fracture Mechanics Test Methods For Sandwich Composites," M.Sc Thesis, University of Utah, Salt Lake City, UT, 2009.
- [5] Cantwell W.J., and Davies P., "A Study of Skin-Core Adhesion in Glass Fiber Reinforced Sandwich Materials," *Applied Composite Materials*, Vol. 3, 1996, pp. 407-420.
- [6] Cantwell W.J., Scudamore R., Ratcliffe J., and Davies P., "Interfacial Fracture in Sandwich Laminates," *Composites Science and Technology*, Vol. 54, No. 14, 1999, pp. 2079-2085.
- [7] McGarva L.D., and Åström B.T., "Experimental Investigation of Compression Moulding of Glass/PA12-PMI foam Core Sandwich Components," *Composites: Part A*, Vol. 30, 1999, pp. 1171-1185.
- [8] Shivakumar K., Chen H., and Smith S.A., "An Evaluation of Data Reduction Methods for Opening Mode Fracture Toughness of Sandwich Panels," *Journal of Sandwich Structure and Materials*, Vol. 4, No. 1, 2005, pp. 77-90.
- [9] Cantwell W.J., Broster G., and Davies P., "The Influence of Water Immersion on Skin-Core Debonding in GFRP-Balsa Sandwich Structures," *Journal of Reinforced Plastics, and Composites*, Vol. 15, 1996, pp. 1161-1172.
- [10] Li X., and Carlsson L.A., "The Tilted Sandwich Debond (TSD) Specimen for Face/Core Interface Fracture Characterization," *Journal of Sandwich Structures and Materials*, Vol. 1, 1999, pp. 60-75.

- [11] Cantwell W.J., and Davies P., “A Test Technique For Assessing Core-Skin Adhesion in Composite Sandwich Structures,” *Journal of Materials Science Letters*, Vol. 13, 1994, pp. 203-205.
- [12] Glaessgen E.H., Reeder J.R., Sleight D.W., Wang J.T., Raju I.S., and Harris C.E., “Debonding Failure of Sandwich-Composite Cryogenic Fuel Tank with Internal Core Pressure,” *Journal of Spacecraft and Rockets*, Vol. 42, No. 4, 2005, pp. 613-627.
- [13] Prasad S, and Carlsson L.A., “Debonding and Crack Kinking in Foam Core Sandwich Beams–II. Experimental Investigation,” *Engineering Fracture Mechanics*, Vol. 47, No. 6, 1994, pp. 825-841.
- [14] Smith S.A., and Shivakumar K.N., “Modified Mode-I Cracked Sandwich Beam (CSB) Fracture Test,” *Proceedings of the AIAA/ASME/ASCE/AHS/ASC Structures, Structural Dynamics and Materials Conference*, Vol. 1, 2001, AIAA, Reston, VA, pp. 1-18.
- [15] Østergaard R.C., and Sørensen B.F., “Interface Crack in Sandwich Specimen,” *International Journal of Fracture*, 2007, Vol. 143, pp. 301-316.
- [16] Shivakumar K.N., and Smith S.A., “In Situ Fracture Toughness Testing of Core Materials in Sandwich Panels,” *Journal of Composite Materials*, Vol. 38, No. 8, 2004, pp. 655-668.
- [17] Gates T.S., and Herring H.M., “Facesheet Push-off Tests to Determine Composite Sandwich Toughness at Cryogenic Temperatures,” *Proceedings of the AIAA/ASME/ASCE/AHS/ASC Structures, Structural Dynamics and Materials Conference*, Vol. 1, 2001, AIAA, Reston, VA, pp. 323-333.
- [18] Ratcliffe J., and Cantwell W.J., “A New Test Geometry for Characterizing Skin-Core Adhesion in Thin-Skinned Sandwich Structures,” *Journal of Materials Science Letters*, Vol. 19, 2000, pp. 1365-1367.
- [19] Berggreen C., Simonsen B.C., and Borum K.K., “Experimental and Numerical Study of Interface Crack Propagation in Foam-Cored Sandwich Beams,” *Journal of Composite Materials*, Vol. 41, No. 4, 2007, pp. 493-520.
- [20] Shipsha A., Burman M., and Zenkert D., “Interfacial Fatigue Crack Growth in Foam Core Sandwich Structures,” *Fatigue and Fracture of Engineering Materials and Structures*, Vol. 22, 1999, pp. 123-131.
- [21] Ural A., Zehnder A.T., and Ingrassia A.R., “Fracture Mechanics Approach to Facesheet Delamination in Honeycomb: Measurement of Energy Release Rate of Adhesive Bond,” *Engineering Fracture Mechanics*, Vol. 70, 2003, pp. 93-103.
- [22] Li X., and Carlsson L.A., “Elastic Foundation Analysis of Tilted Sandwich Debond (TSD) Specimen,” *Journal of Sandwich Structures and Materials*, Vol. 2, 2000, pp. 3-32.
- [23] Carlsson L.A., Sendlein L.S., and Merry S.L., “Characterization of Face Sheet/Core Shear Fracture of Composite Sandwich Beams,” *Journal of Composite Materials*, Vol. 25, 1991, pp. 101-116.
- [24] Quispitupa A., Berggreen C., Carlsson LA, A “Debond Sandwich Specimen Under Mixed Mode Bending (MMB),” In: *Proceedings of the 8th international conference on sandwich structures*, Porto, Portugal, 2008, pp. 186–98.
- [25] Quispitupa A, Berggreen C, Carlsson LA. “On The Analysis of a Mixed Mode Bending Sandwich Specimen for Debond Fracture Characterization,” *Engineering Fracture Mechanics*, Vol. 76, 2009, pp. 594–613.

- [26] Rinker M., John M., Zahlen P.C., Schäuble R., “Face Sheet Debonding in CFRP/PMI Sandwich Structures Under Quasi-Static and Fatigue Loading Considering Residual Thermal Stress,” *Engineering Fracture Mechanics*, Vol. 78, Issue 17, 2011, pp. 2835-2847.
- [27] Ratcliffe JG. “Sizing Single Cantilever Beam Specimens for Characterizing Facesheet/Core Peel Debonding in Sandwich Structure, NASA Technical Publication, NASA/TP-2010-216169, NASA Langley Research Center, Hampton, Virginia 23681-2199, USA; 2010.
- [28] Ratcliffe JG. Sizing Single Cantilever Beam Specimens for Characterizing Facesheet/Core Peel Debonding in Sandwich Structure. In: *Proceedings of the 9th International Conference on Sandwich Structures*, LA, CA, USA; 2010.
- [29] Adams, D. and Ratcliffe, J.G., 2012, “Development and Evaluation of Fracture Mechanics Test Methods,” CMH-17 Sandwich Debond/Delam Task Group Meeting for Sandwich Composites, Boston, MA.
- [30] Ley Richardson, DuPont. Private communications.
- [31] Nomex HRH-10-3/16-3, Hexcel Corporation, Salt Lake City, UT.
- [32] M30SC 18K/1915;40;165AW Unidirectional Carbon Fiber Prepreg, Hexcel Corporation, Salt Lake City, UT.
- [33] FM-300-1, Cytotec Industries Inc., West Paterson, NJ.
- [34] American Society for Testing and Materials, “Standard Test Method for Mode I Interlaminar Fracture Toughness of Unidirectional Fiber-Reinforced Polymer Matrix Composites,” ASTM Standard D5528-01(07), In: *ASTM Annual Book of Standards*, Vol. 15.03, ASTM, 2008.
- [35] Irwin G.R., “A Critical Energy Rate Analysis of Fracture Strength,” *Welding Journal (Research Supplement)*, 1954.
- [36] Kanninen M.F., “An Augmented Double Cantilever Beam Model For Studying Crack Propagation and Arrest,” *International Journal of Fracture*, Vol. 9, No. 1, 1973, pp. 83-92.

Width, mm	Facesheet thickness, mm	Cell size, mm	Initial disbond length, mm	Repeats
25.4	0.95 (6 plies)	0.375	19.0	3
25.4	1.90 (12 plies)	0.375	22.2	3
50.8	0.48 (3 plies)	0.375	33.1	4
50.8	0.95 (6 plies)	0.375	18.8 ... 24.5	7
50.8	1.90 (12 plies)	0.375	21.7	3
76.2	0.95 (6 plies)	0.375	22.3	3
76.2	1.90 (12 plies)	0.375	20.6	3
50.8	0.95 (6 plies)	0.125	24.6	7
50.8	0.95 (6 plies)	0.188	25.1	9
50.8	0.95 (6 plies)	0.250	22.7	8

Table 1: Matrix of SCB specimens tested.

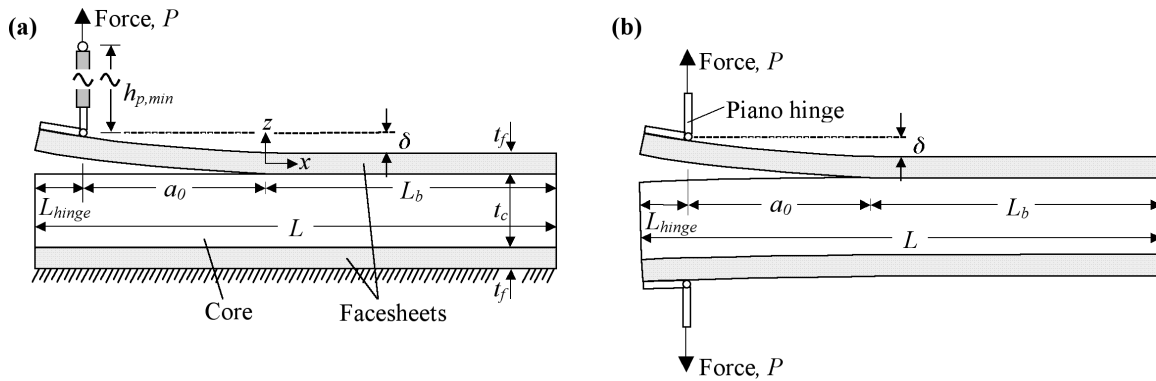


Figure 1 Schematics of facesheet/core disbond specimens. (a) Single cantilever beam configuration, (b) Double cantilever beam configuration.

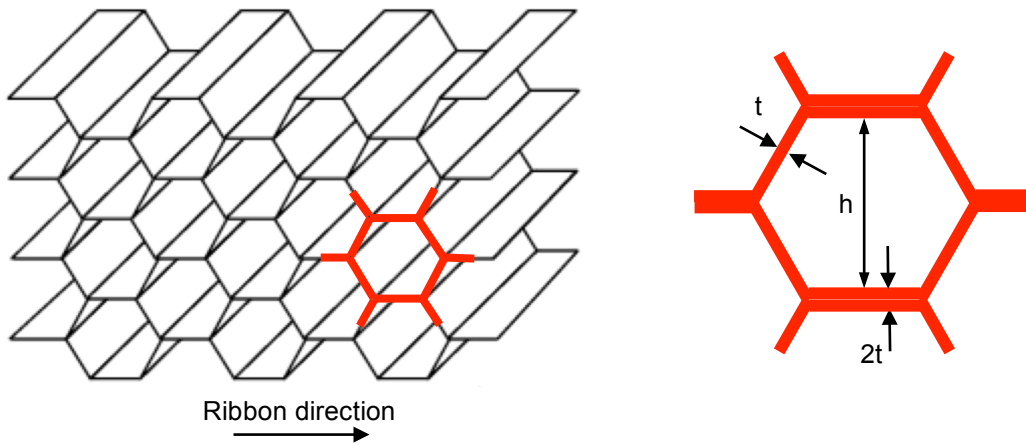


Figure 2 Hexagonal cell geometry of a honeycomb structure

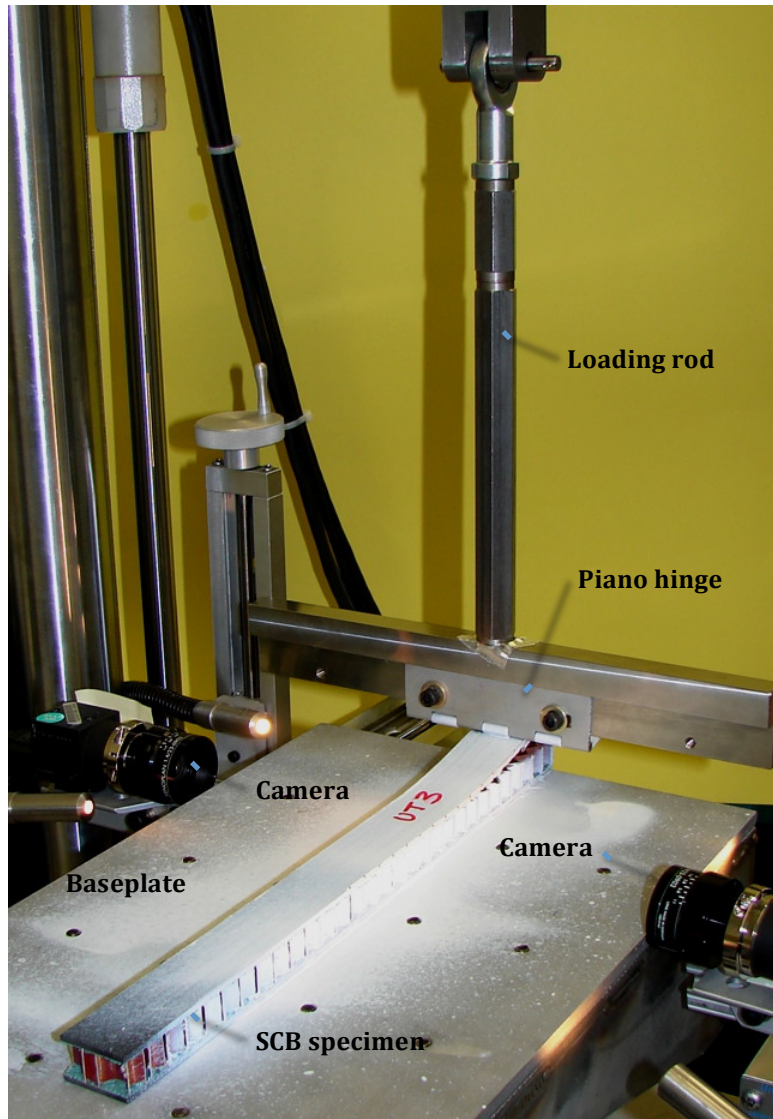


Figure 3 SCB test fixture with loaded specimen.

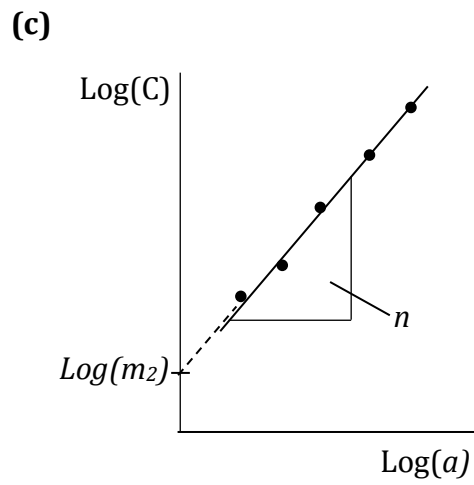
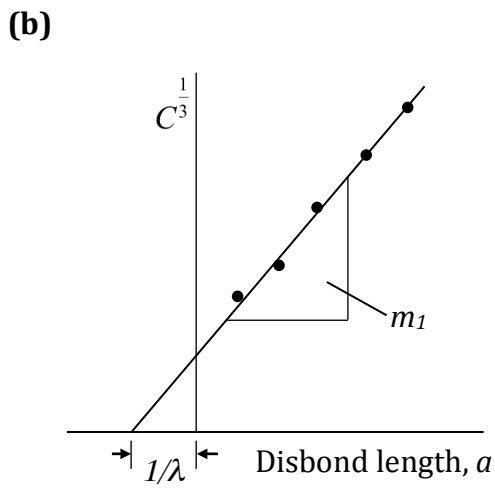
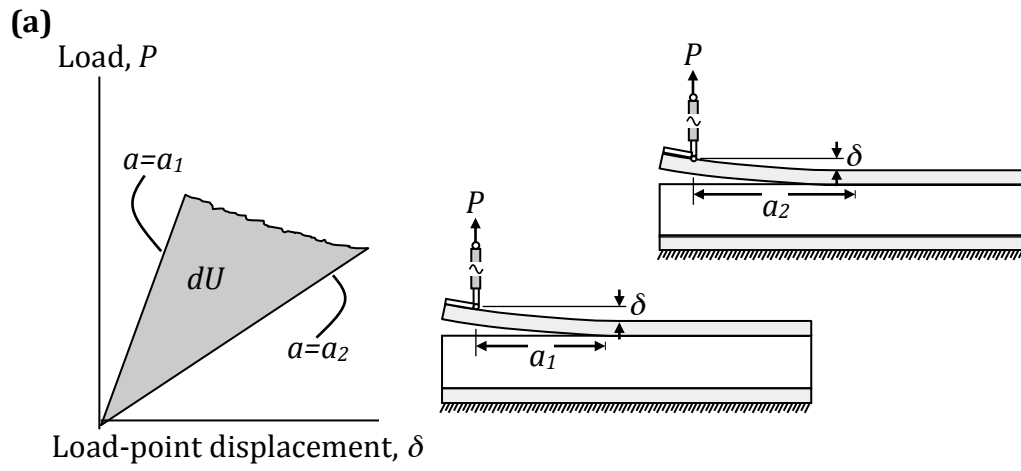


Figure 4: (a) Energy dissipation during disbond growth increment, (b) Plot used to evaluate MBT parameters, m_1 and $1/\lambda$. (c) Plot used to evaluate compliance calibration parameter, n .

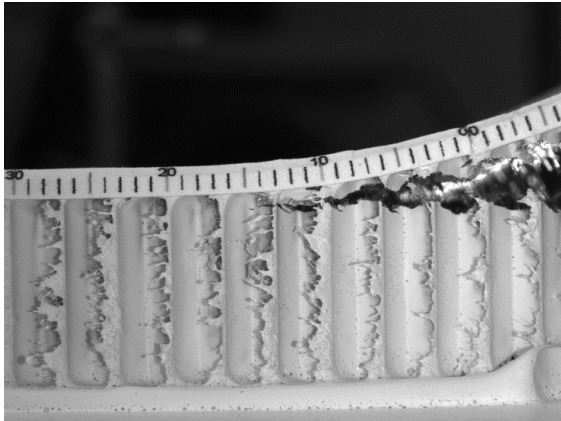


Figure 5: Facesheet disbonding in SCB specimen with 3.2 mm honeycomb cell size.

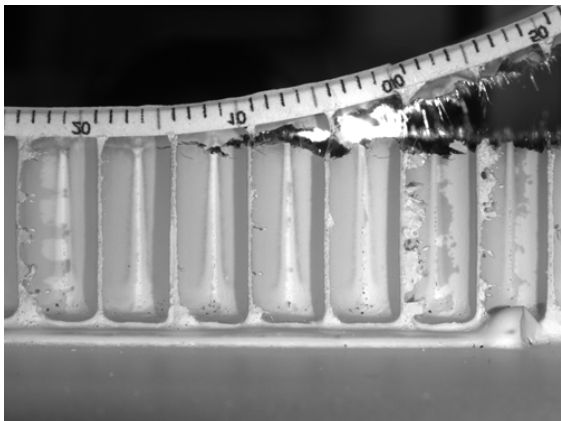
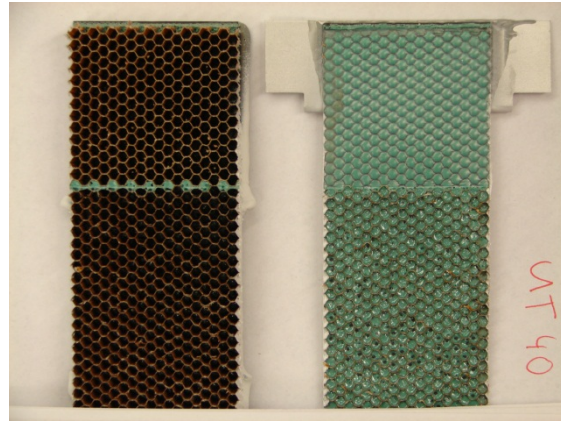


Figure 6: Facesheet disbonding in SCB specimen with 4.8 mm honeycomb cell size.

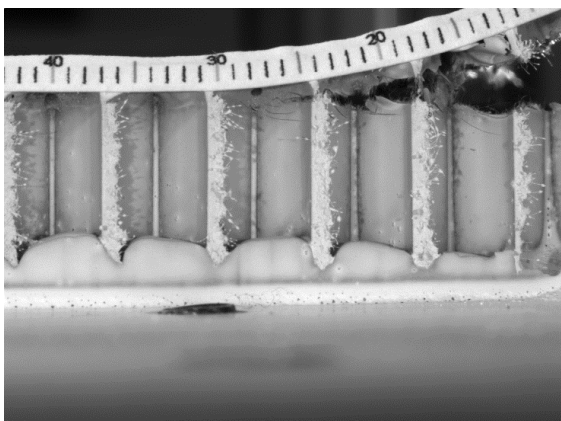
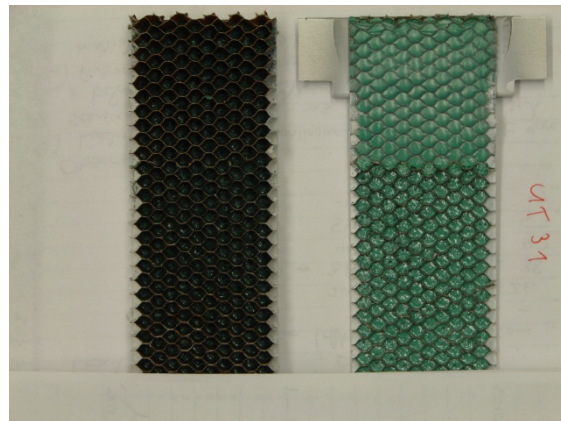
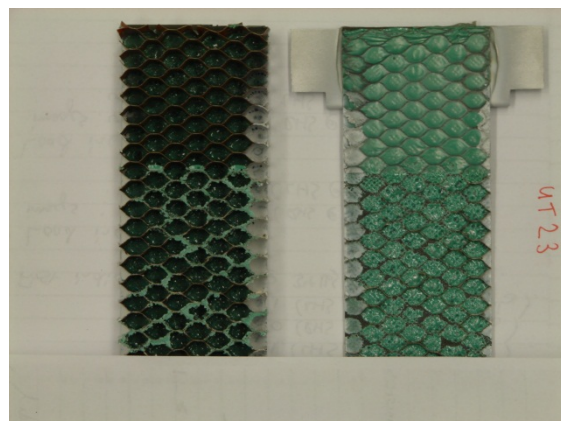


Figure 7: Facesheet disbonding in SCB specimen with 6.4 mm honeycomb cell size.



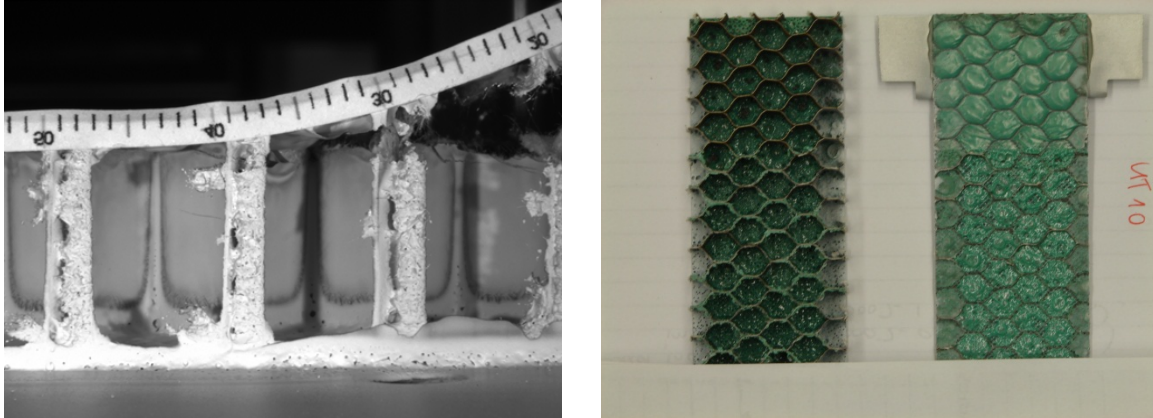


Figure 8: Facesheet disbonding in SCB specimen with 9.5 mm honeycomb cell size.

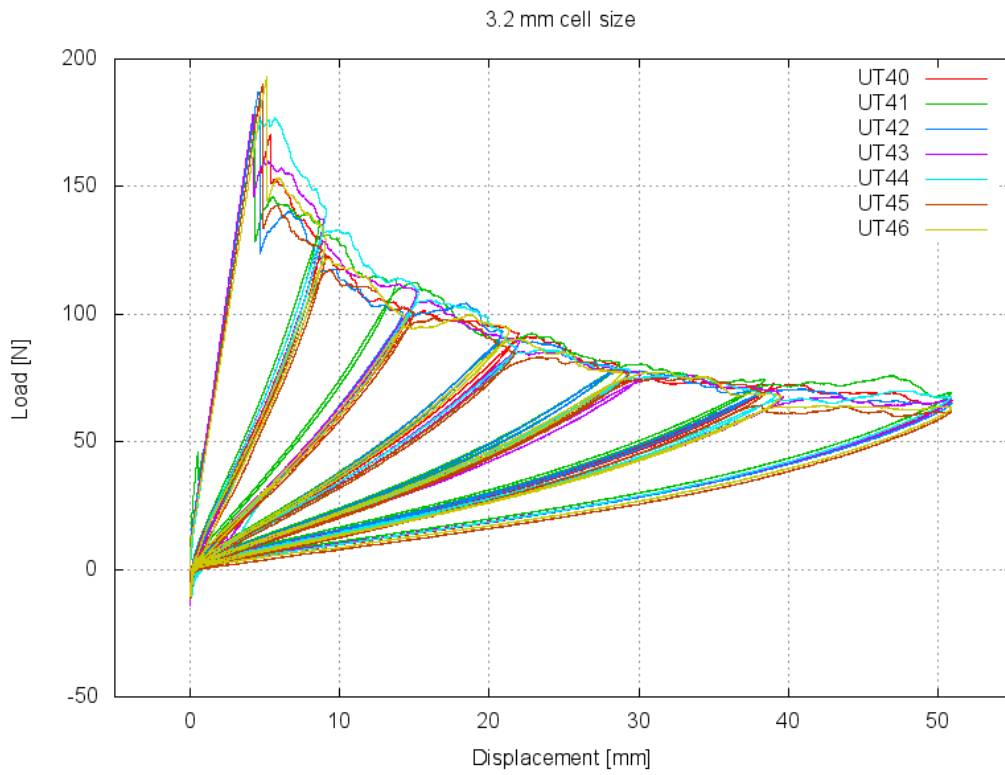


Figure 9: Load-displacement curves of the SCB specimens with 3.2 mm honeycomb cell size.

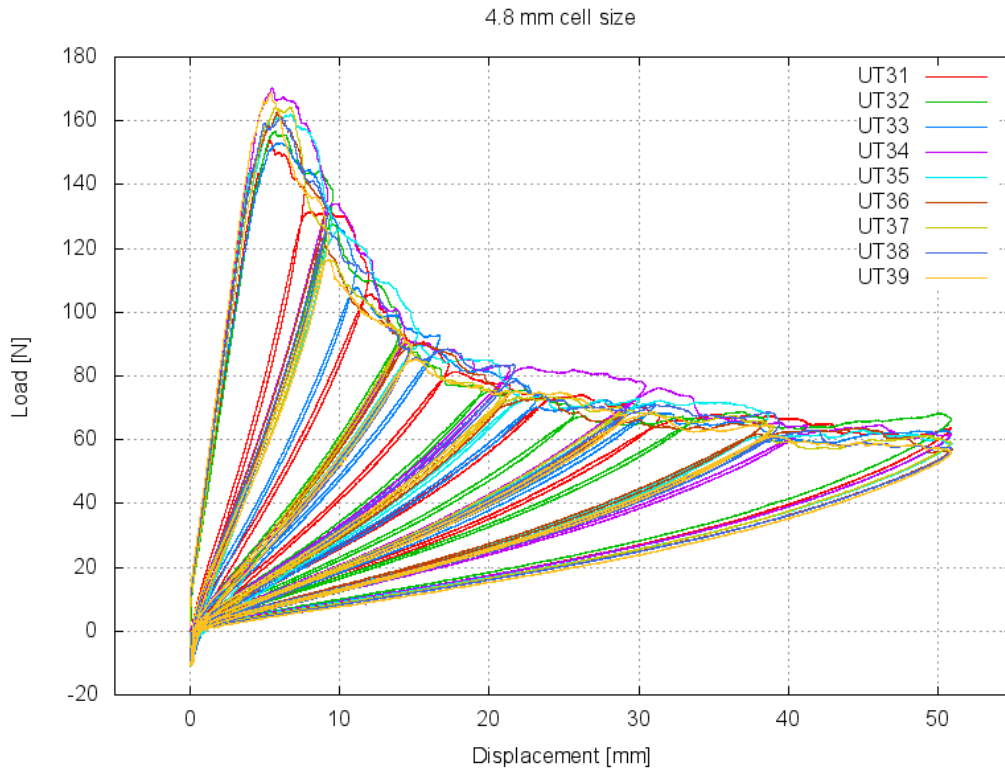


Figure 10: Load-displacement curves of the SCB specimens with 4.8 mm honeycomb cell size.

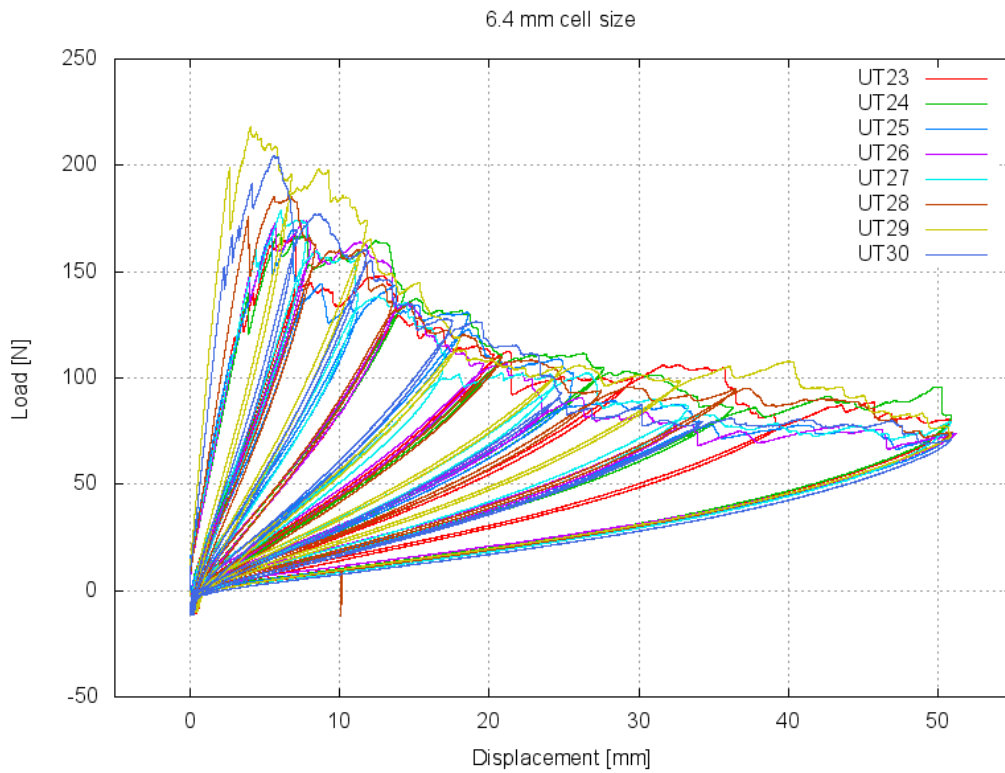


Figure 11: Load-displacement curves of the SCB specimens with 6.4 mm honeycomb cell size.

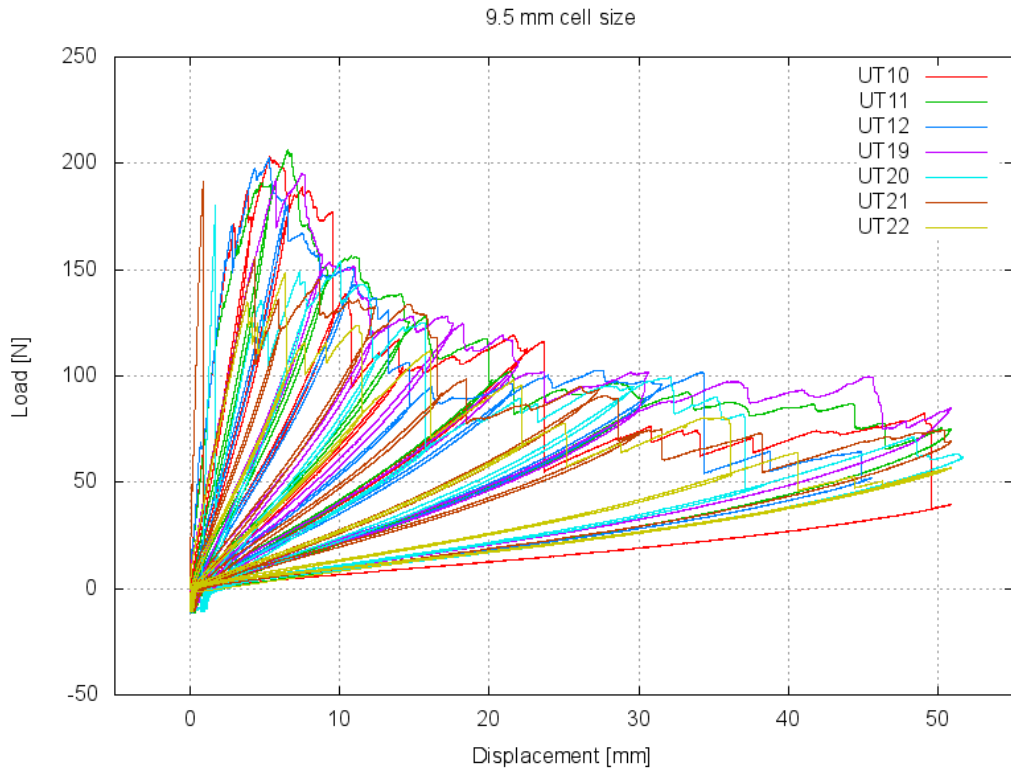


Figure 12: Load-displacement curves of the SCB specimens with 9.5 mm honeycomb cell size.

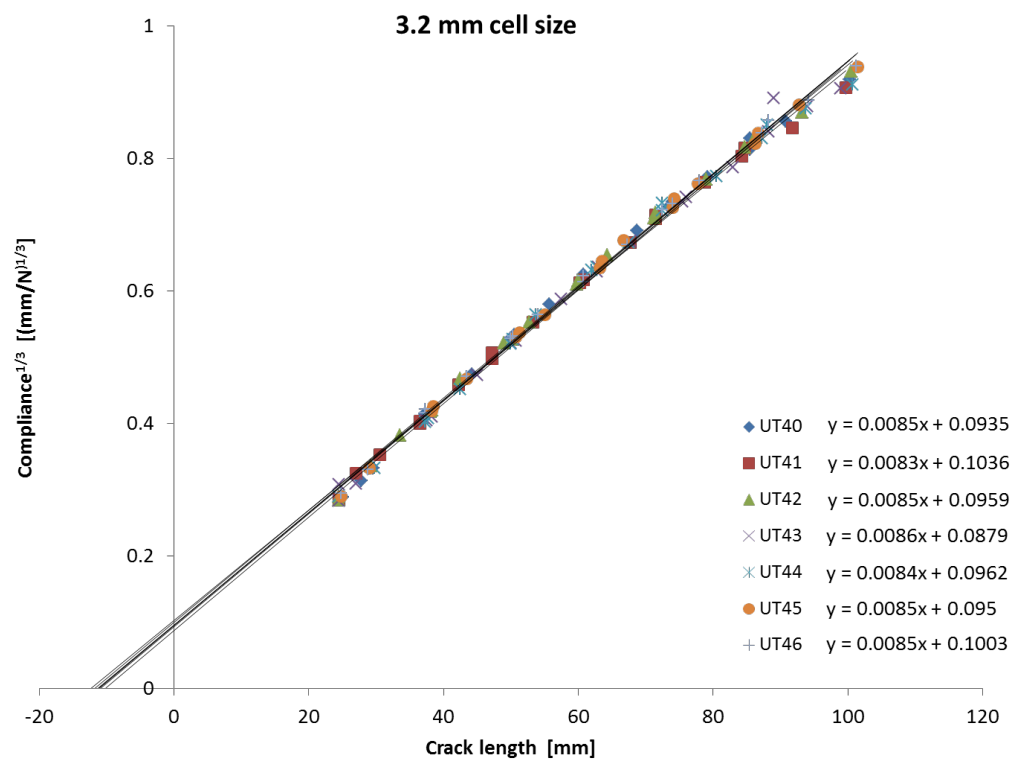


Figure 13: Compliance calibration curves of the SCB specimens with 3.2 mm honeycomb cell size.

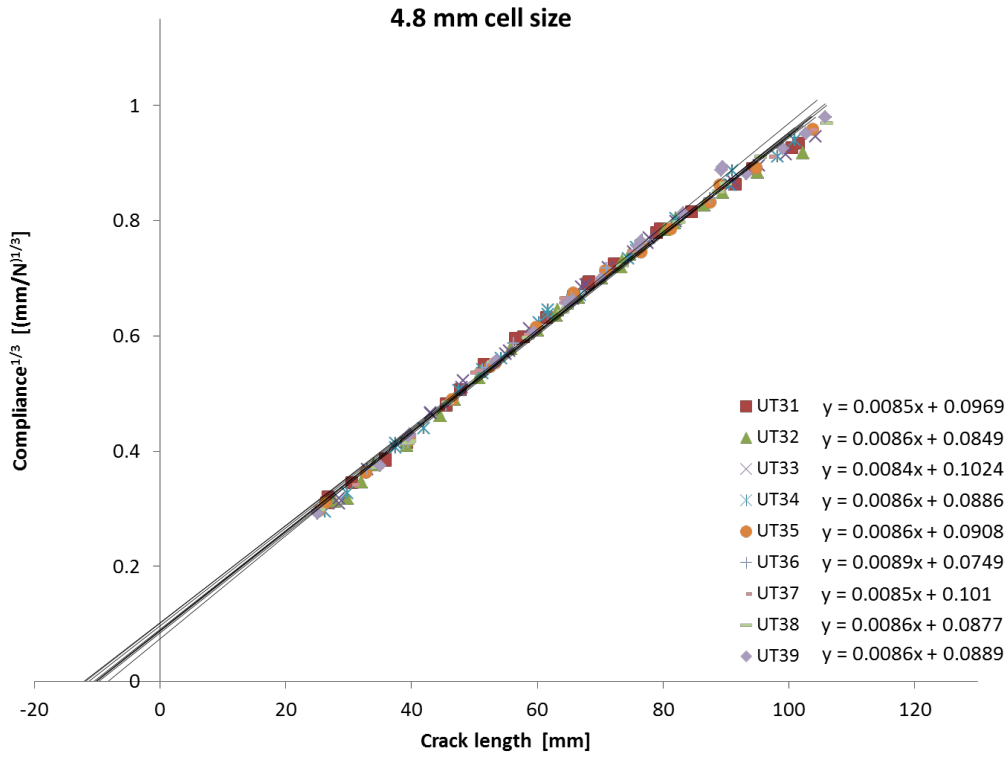


Figure 14: Compliance calibration curves of the SCB specimens with 4.8 mm honeycomb cell size.

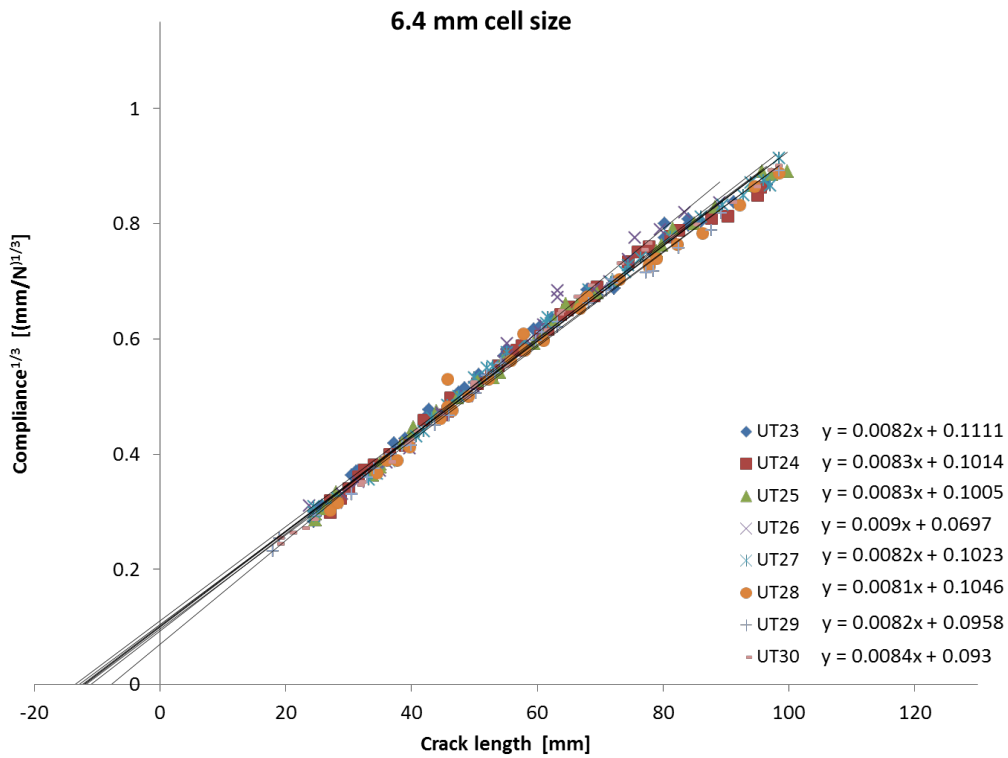


Figure 15: Compliance calibration curves of the SCB specimens with 6.4 mm honeycomb cell size.

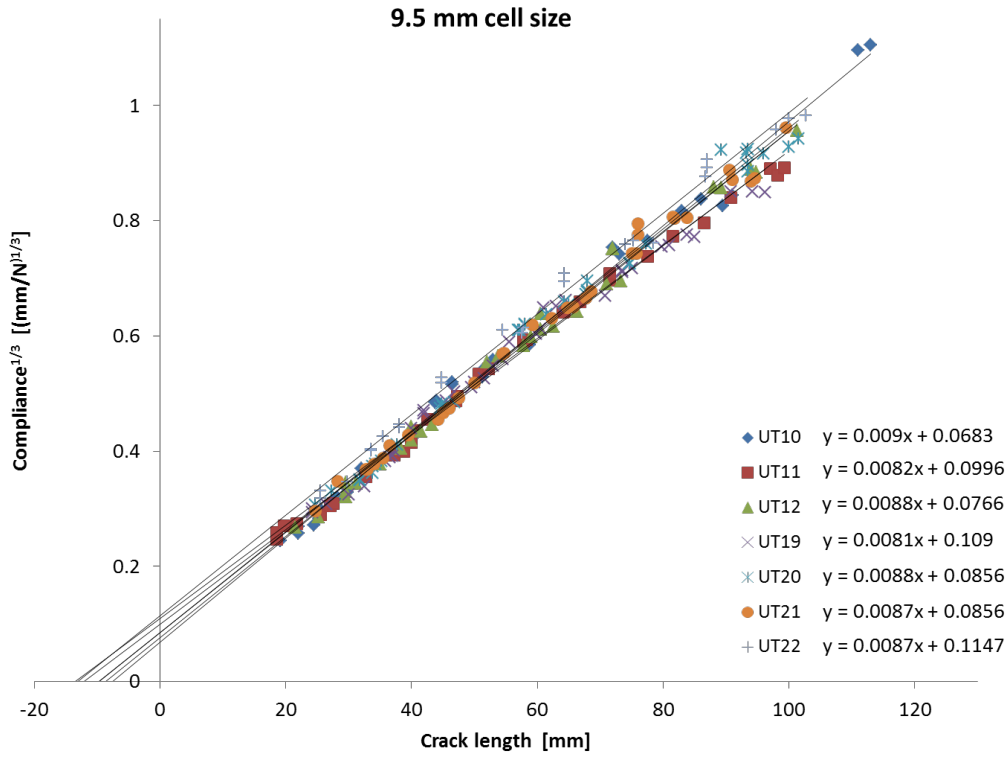


Figure 16: Compliance calibration curves of the SCB specimens with 9.5 mm honeycomb cell size.

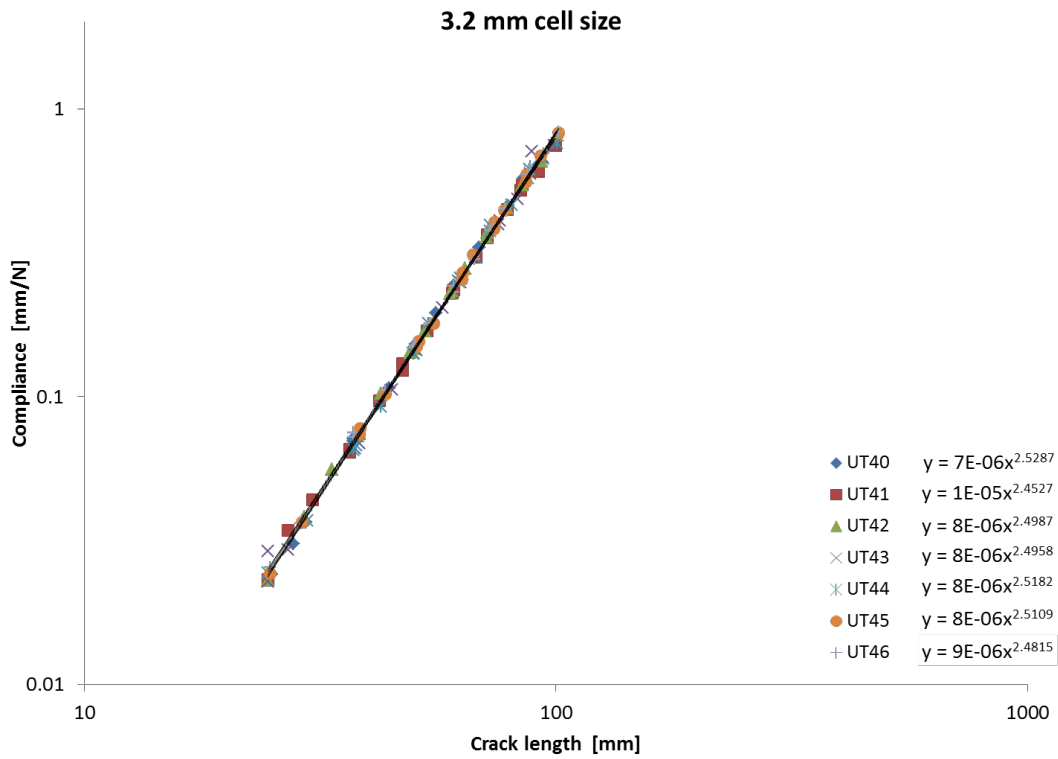


Figure 17: Compliance calibration curves in log-log scale of the SCB specimens with 3.2 mm honeycomb cell size.

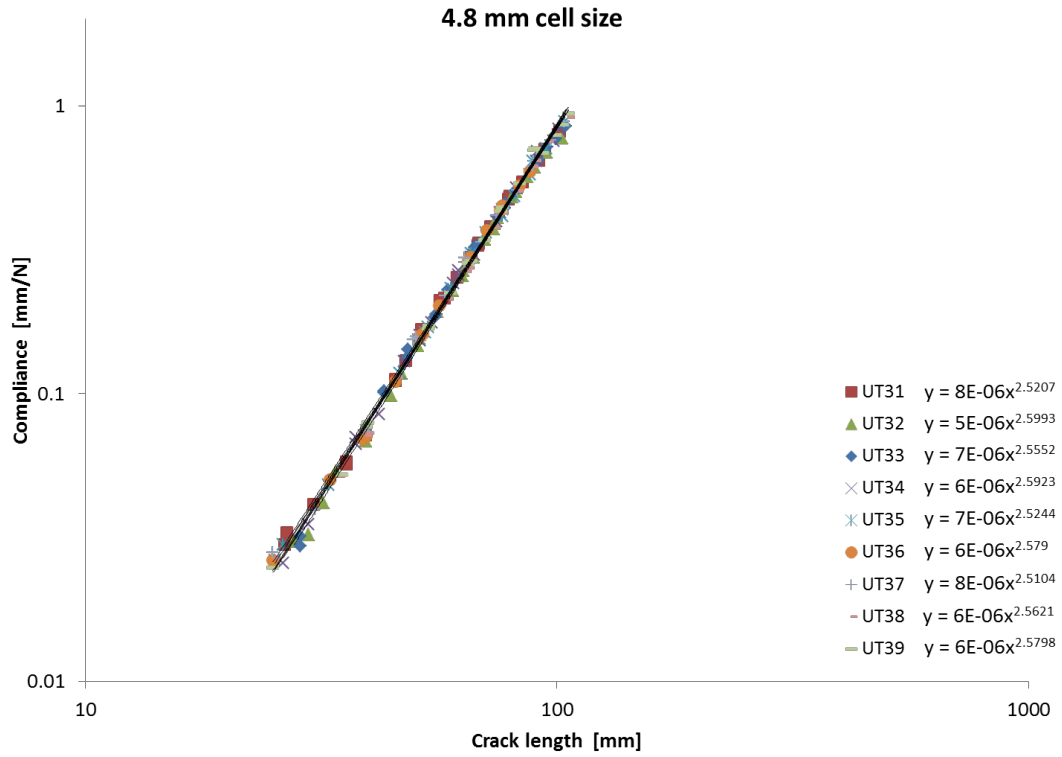


Figure 18: Compliance calibration curves in log-log scale of the SCB specimens with 4.8 mm honeycomb cell size.

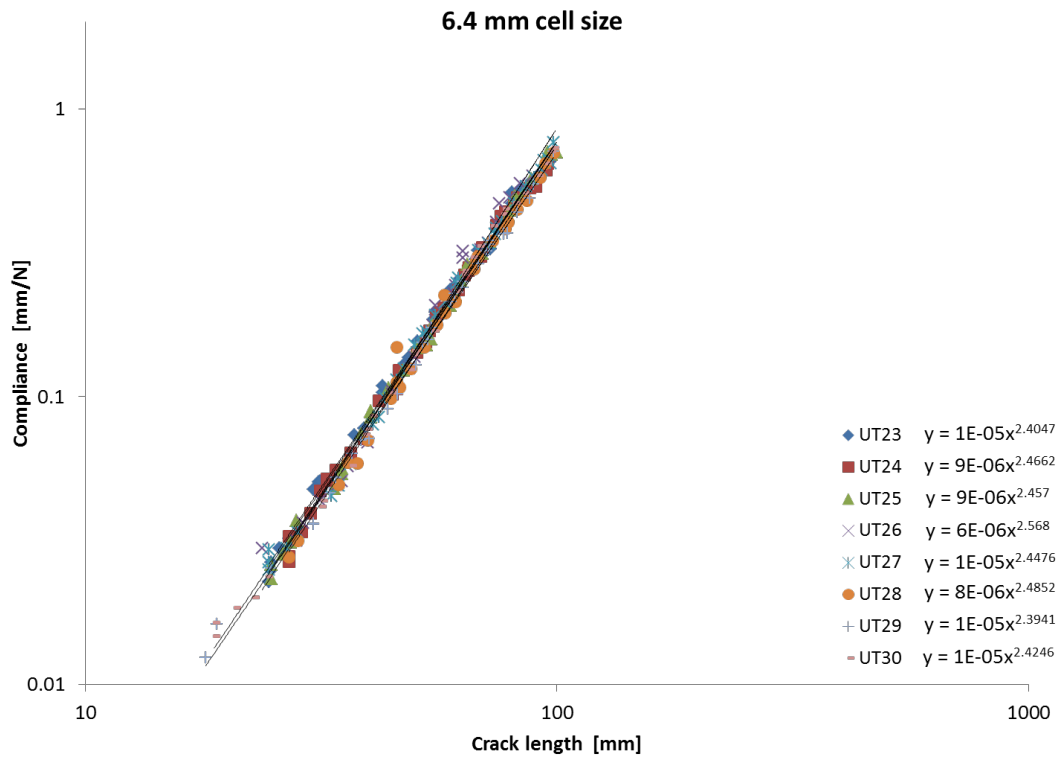


Figure 19: Compliance calibration curves log-log scale of the SCB specimens with 6.4 mm honeycomb cell size.

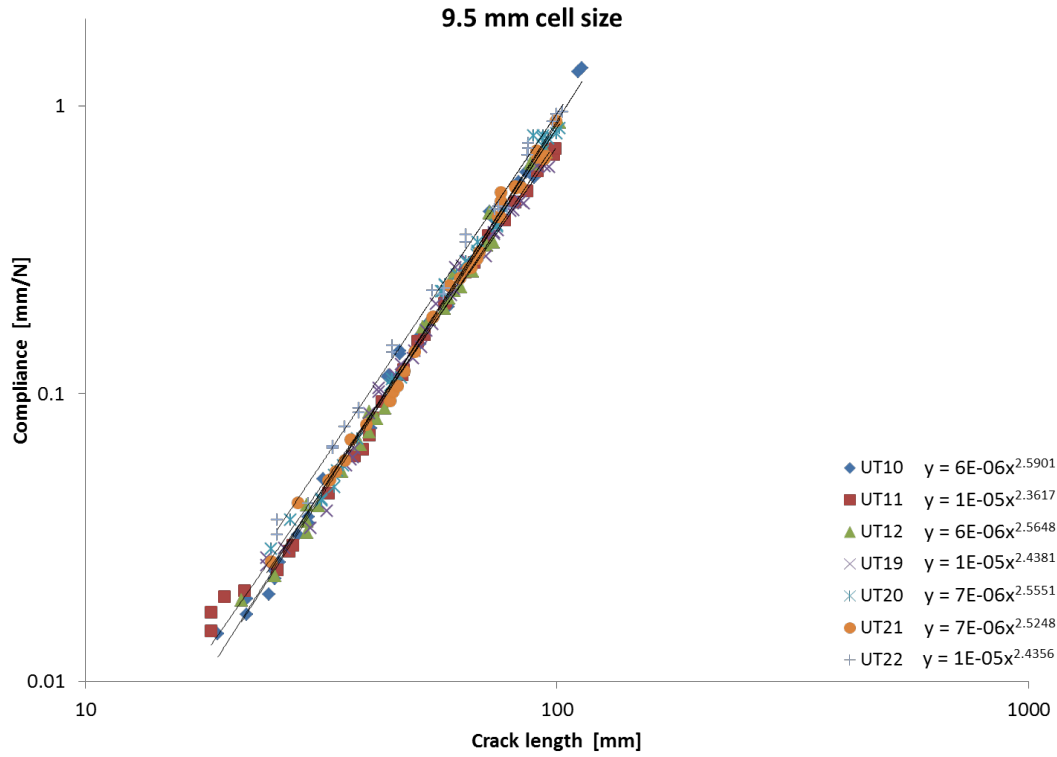


Figure 20: Compliance calibration curves log-log scale of the SCB specimens with 9.5 mm honeycomb cell size.

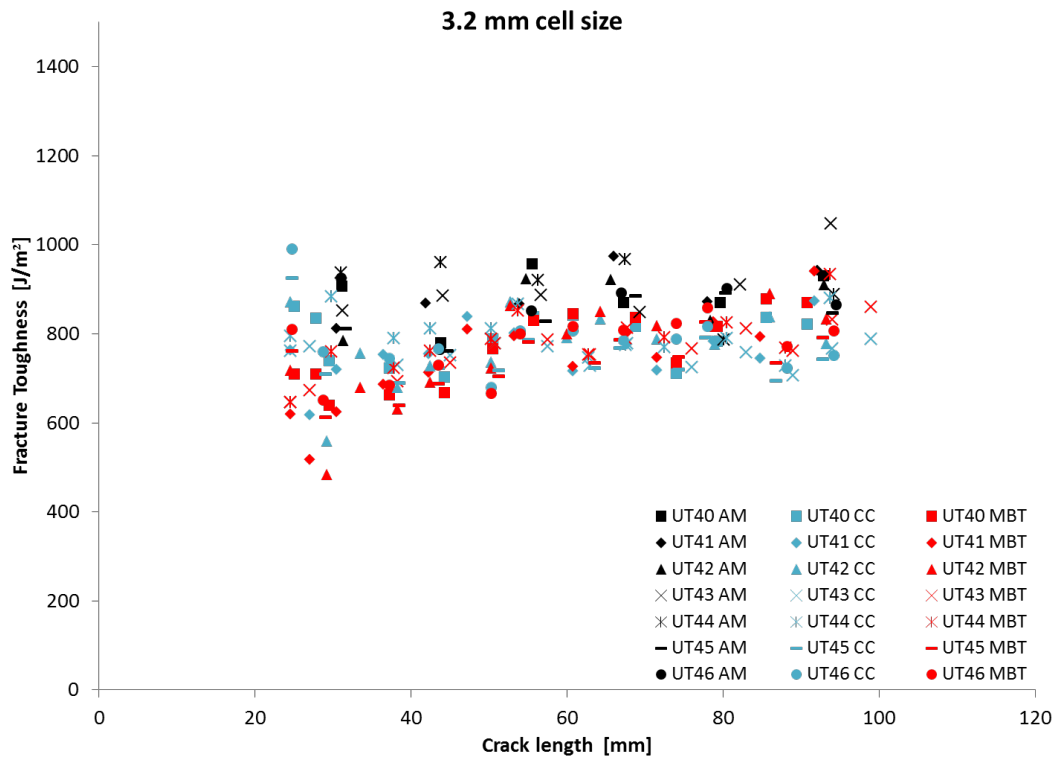


Figure 21: Apparent fracture toughness of the SCB specimens with 3.2 mm honeycomb cell size evaluated via Area Method (AM), Compliance Calibration Method (CC) and Modified Beam Theory (MBT).

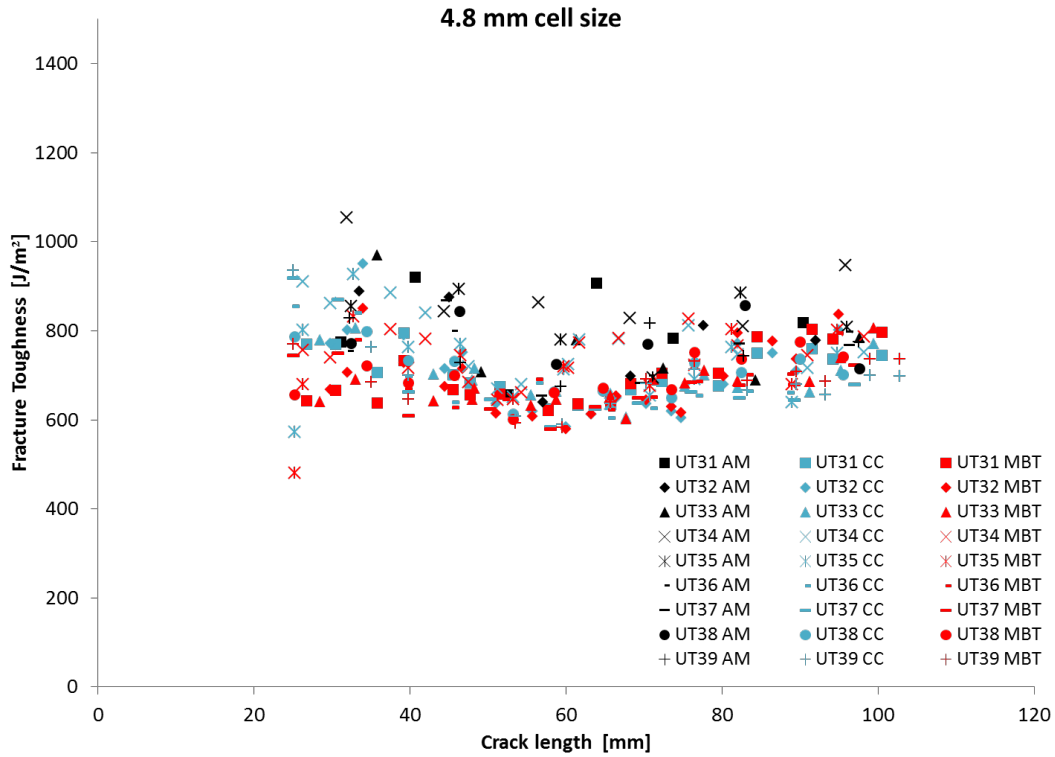


Figure 22: Apparent fracture toughness of the SCB specimens with 4.8 mm honeycomb cell size evaluated via Area Method (AM), Compliance Calibration Method (CC) and Modified Beam Theory (MBT).

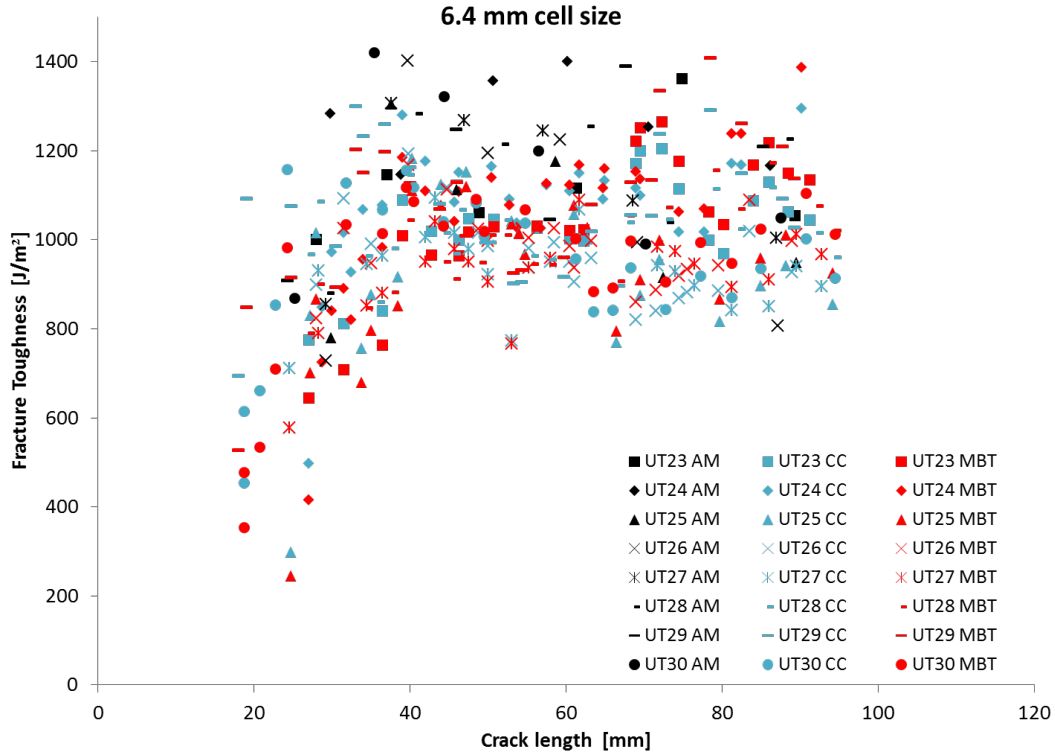


Figure 23: Apparent fracture toughness of the SCB specimens with 6.4 mm honeycomb cell size evaluated via Area Method (AM), Compliance Calibration Method (CC) and Modified Beam Theory (MBT).

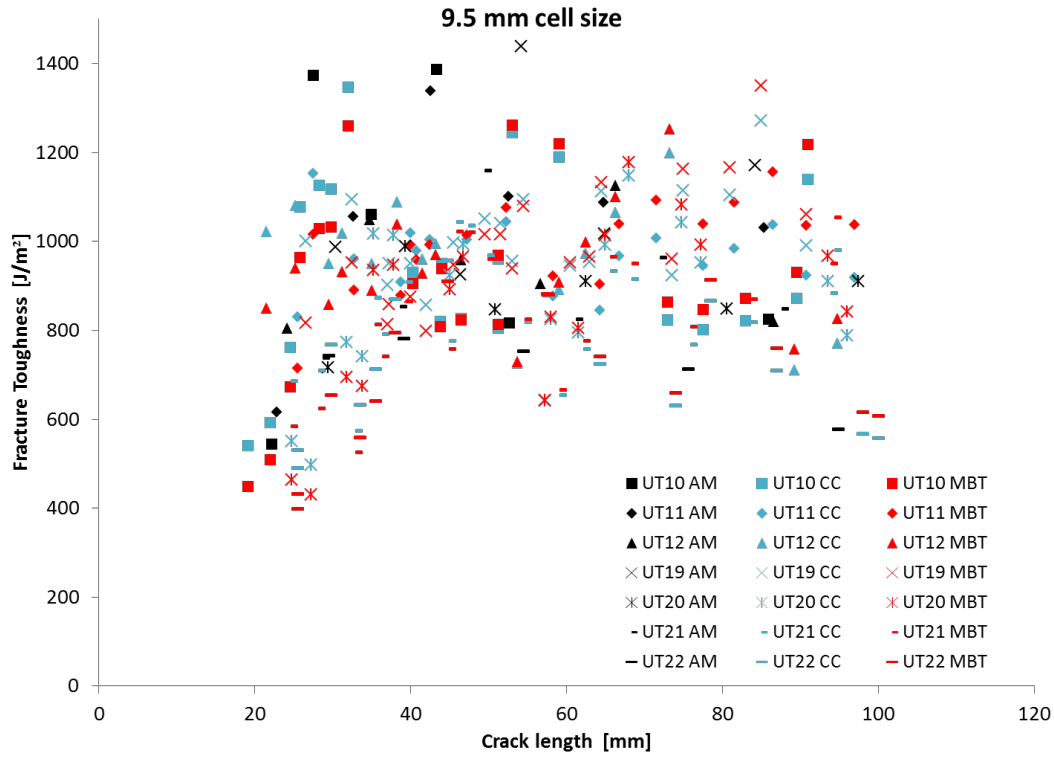


Figure 24: Apparent fracture toughness of the SCB specimens with 9.5 mm honeycomb cell size evaluated via Area Method (AM), Compliance Calibration Method (CC) and Modified Beam Theory (MBT).

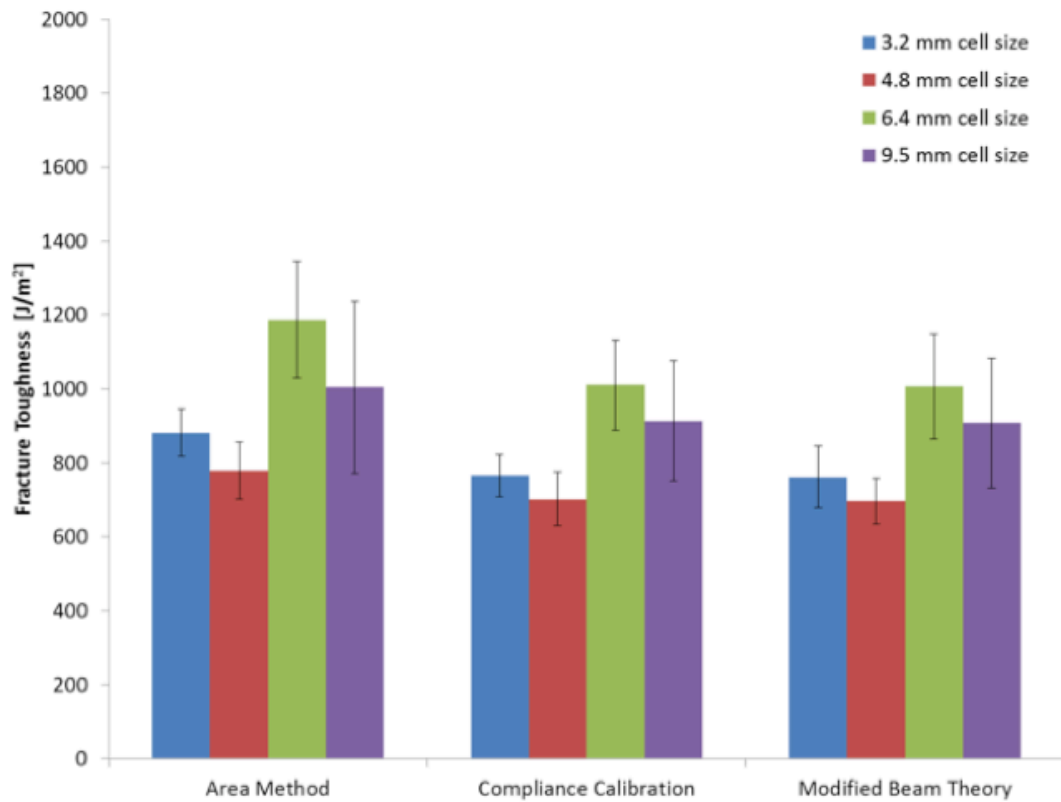


Figure 25: Apparent fracture toughness average of the SCB specimens with different honeycomb cell size.

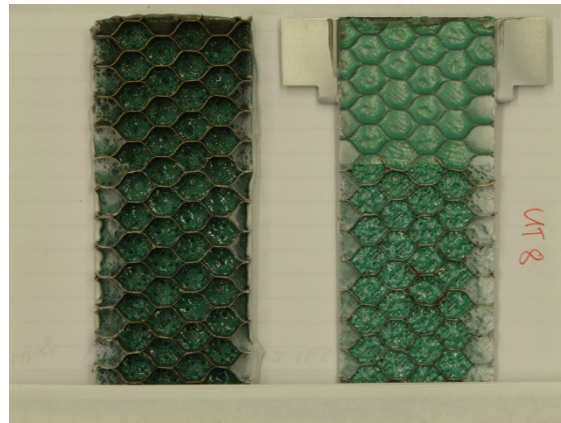
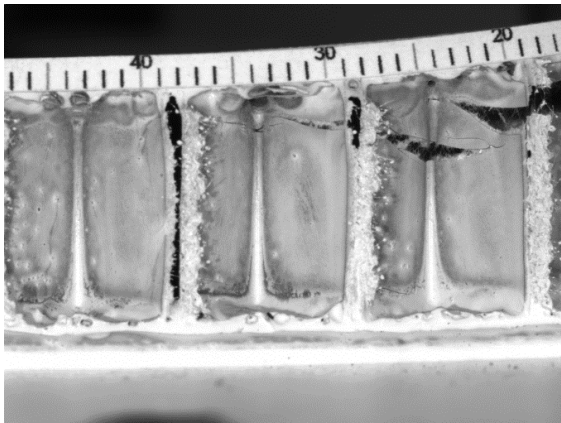


Figure 26: Facesheet disbonding in SCB specimen with 9.5 mm honeycomb cell size and 12-ply facesheets.

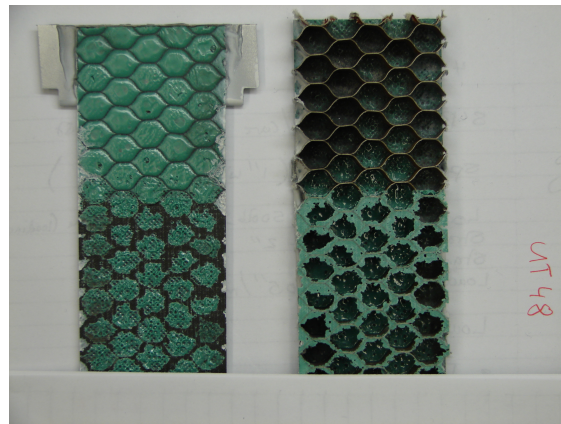
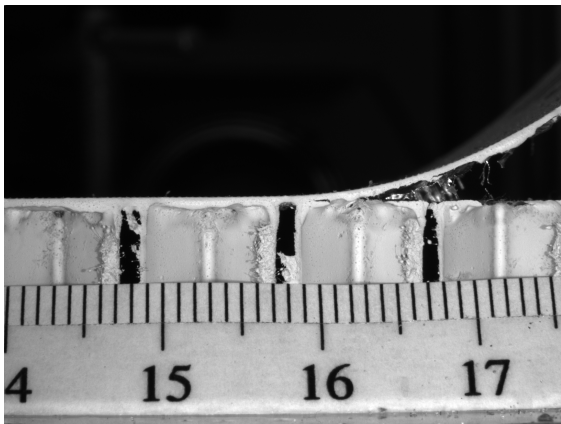


Figure 27: Facesheet disbonding in SCB specimen with 9.5 mm honeycomb cell size and 3-ply facesheets.

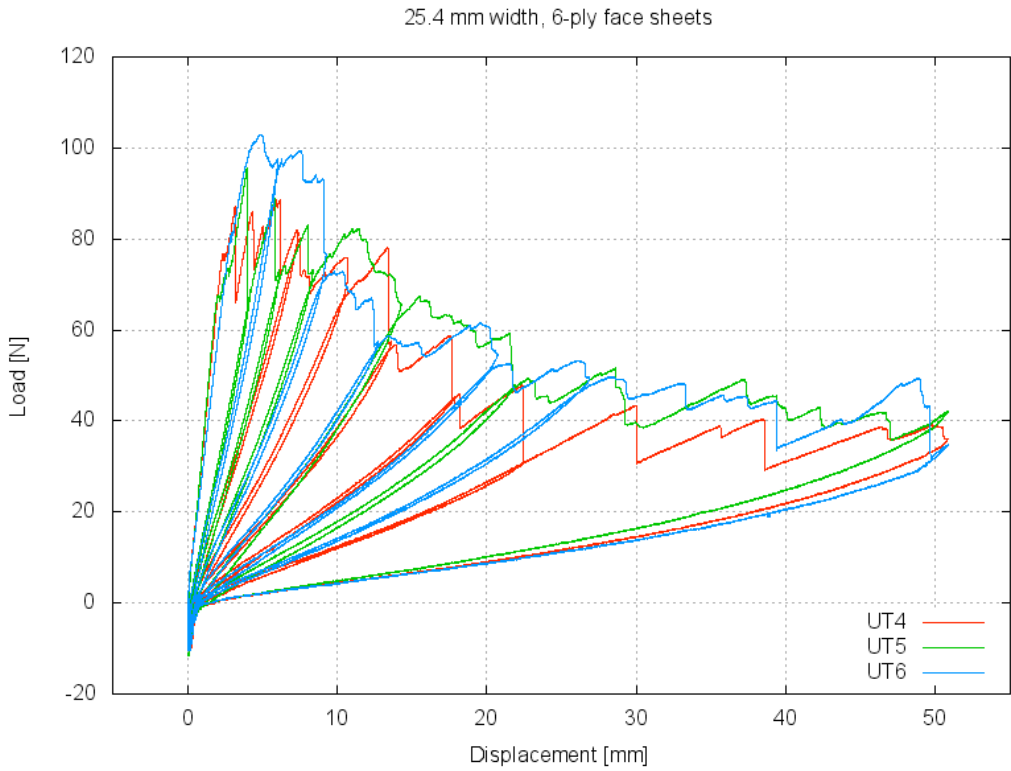


Figure 28: Load-displacement curves of the 25.4 mm wide SCB specimens with 6-ply facesheets.

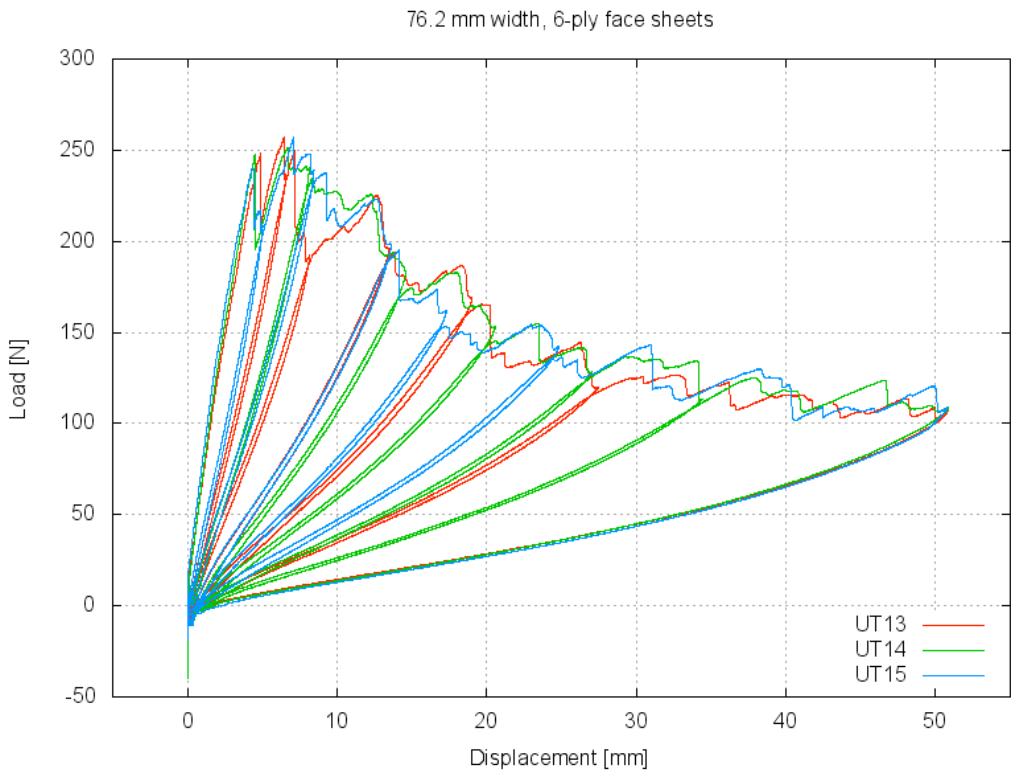


Figure 29: Load-displacement curves of the 76.2 mm wide SCB specimens with 6-ply facesheets.

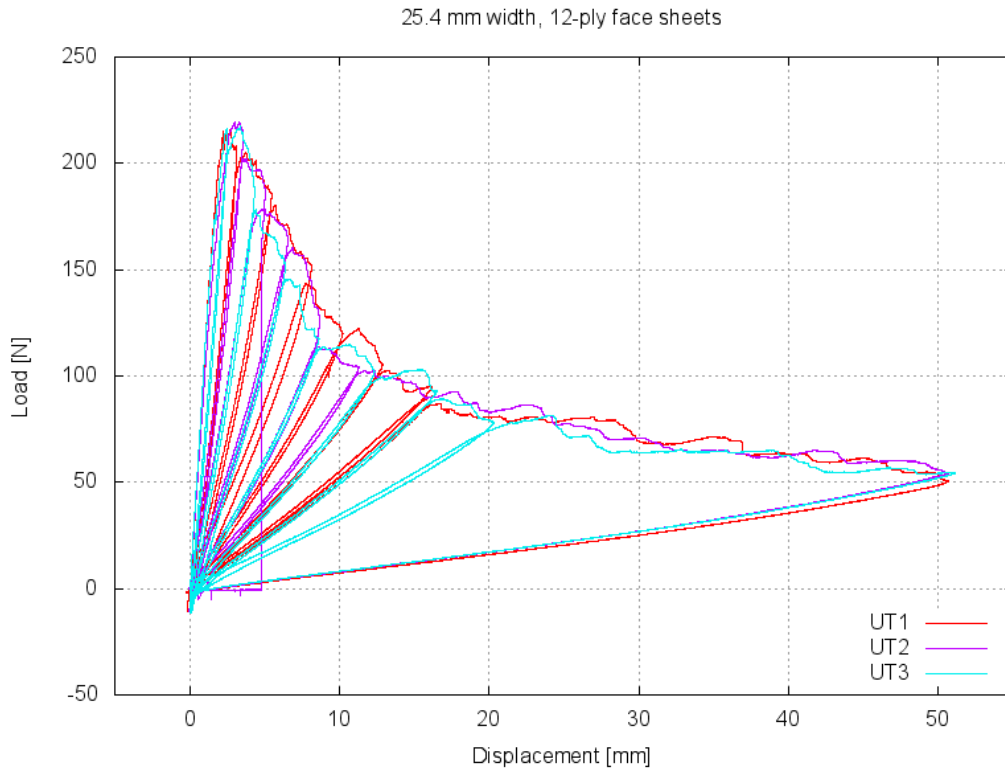


Figure 30: Load-displacement curves of the 25.4 mm wide SCB specimens with 12-ply facesheets.

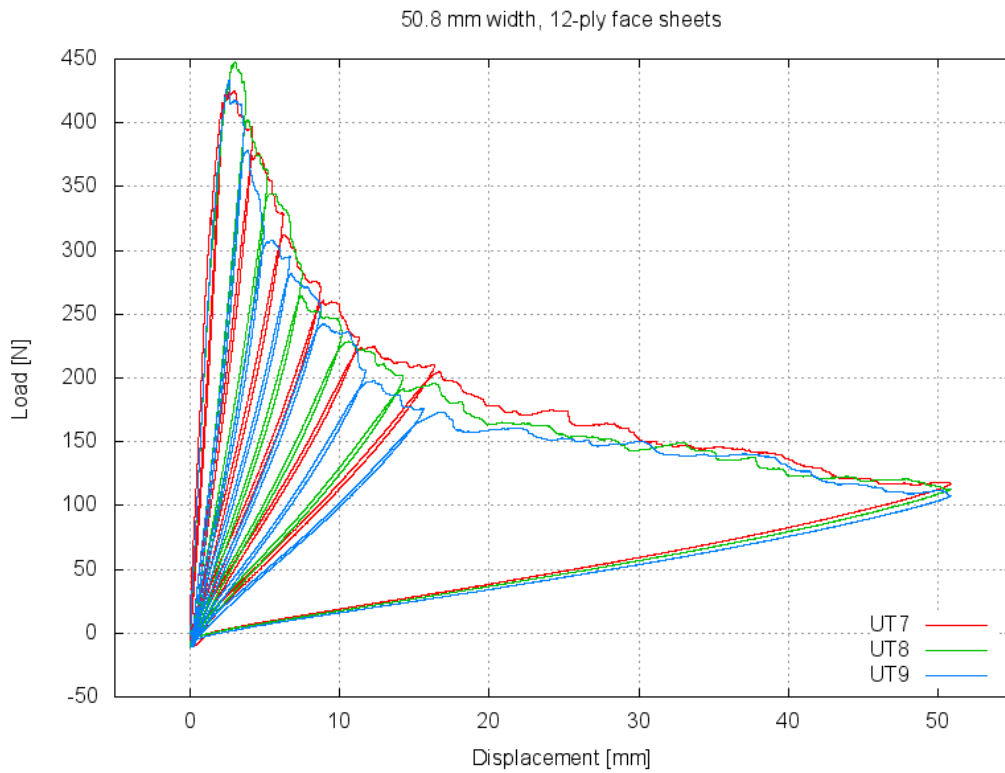


Figure 31: Load-displacement curves of the 50.8 mm wide SCB specimens with 12-ply facesheets.

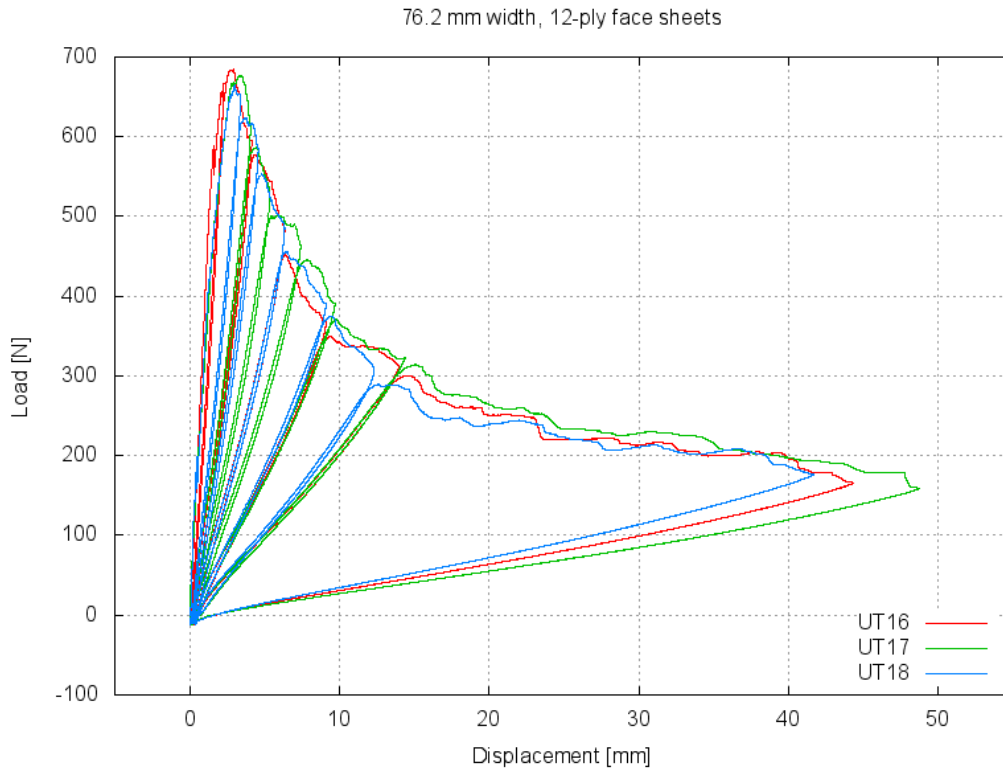


Figure 32: Load-displacement curves of the 76.2 mm wide SCB specimens with 12-ply facesheets.

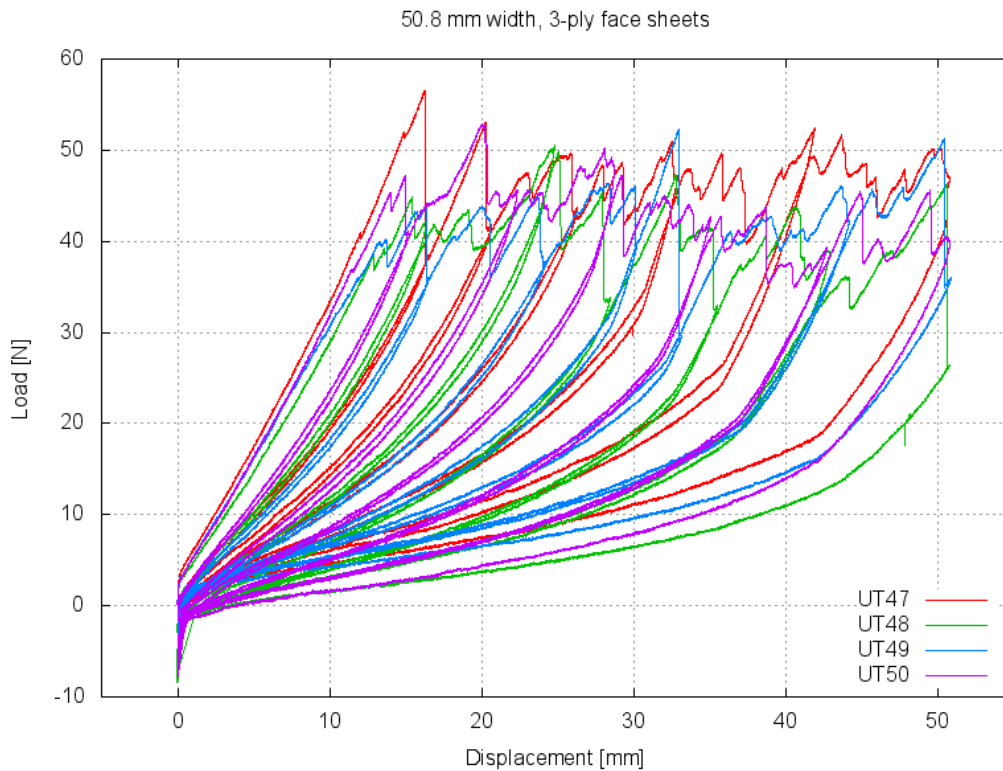


Figure 33: Load-displacement curves of the 50.8 mm wide SCB specimens with 3-ply facesheets.

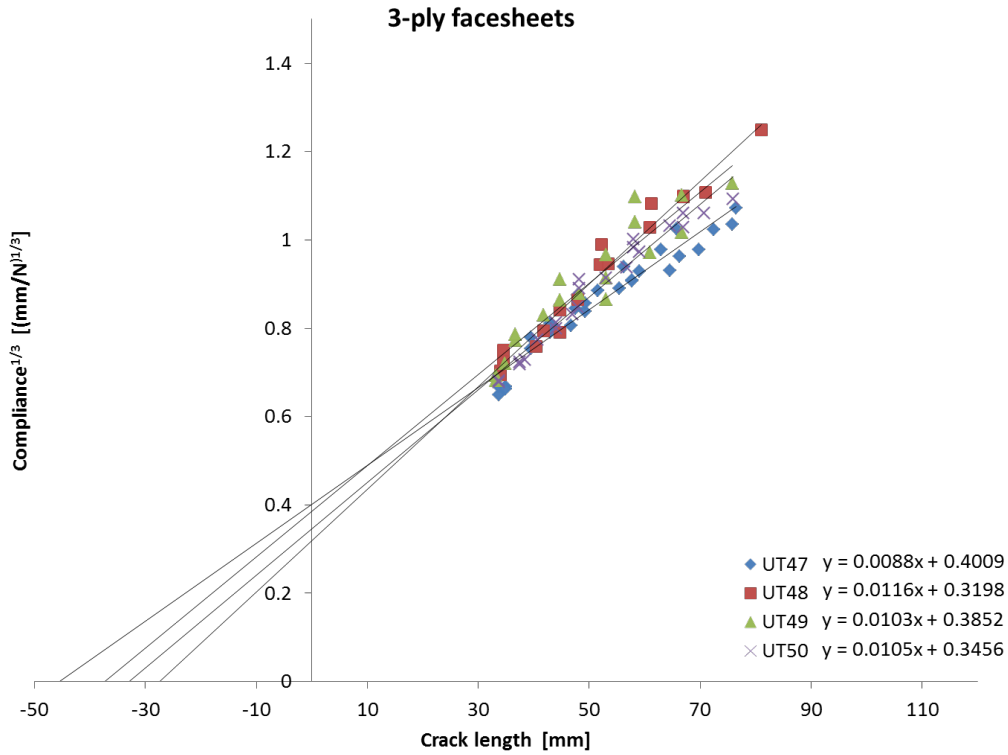


Figure 34: Compliance calibration curves of the SCB specimens with 3-ply facesheets.

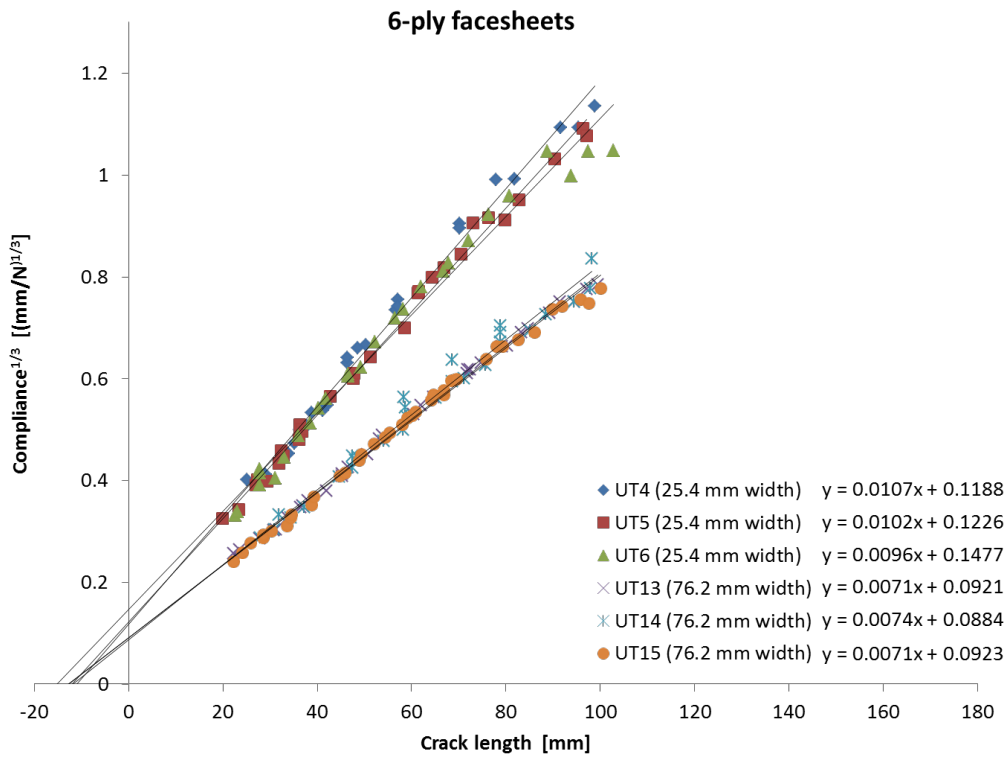


Figure 35: Compliance calibration curves of the 25.4 and 76.2 mm wide SCB specimens with 6-ply facesheets.

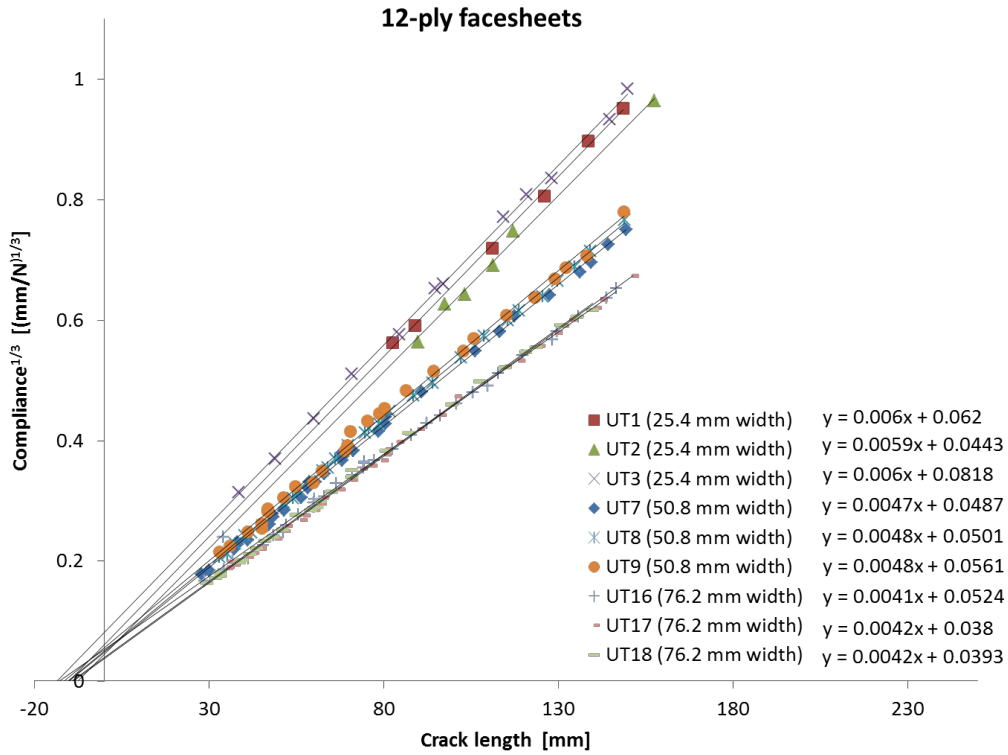


Figure 36: Compliance calibration curves of the 25.4, 50.8 and 76.2 mm wide SCB specimens with 12-ply facesheets.

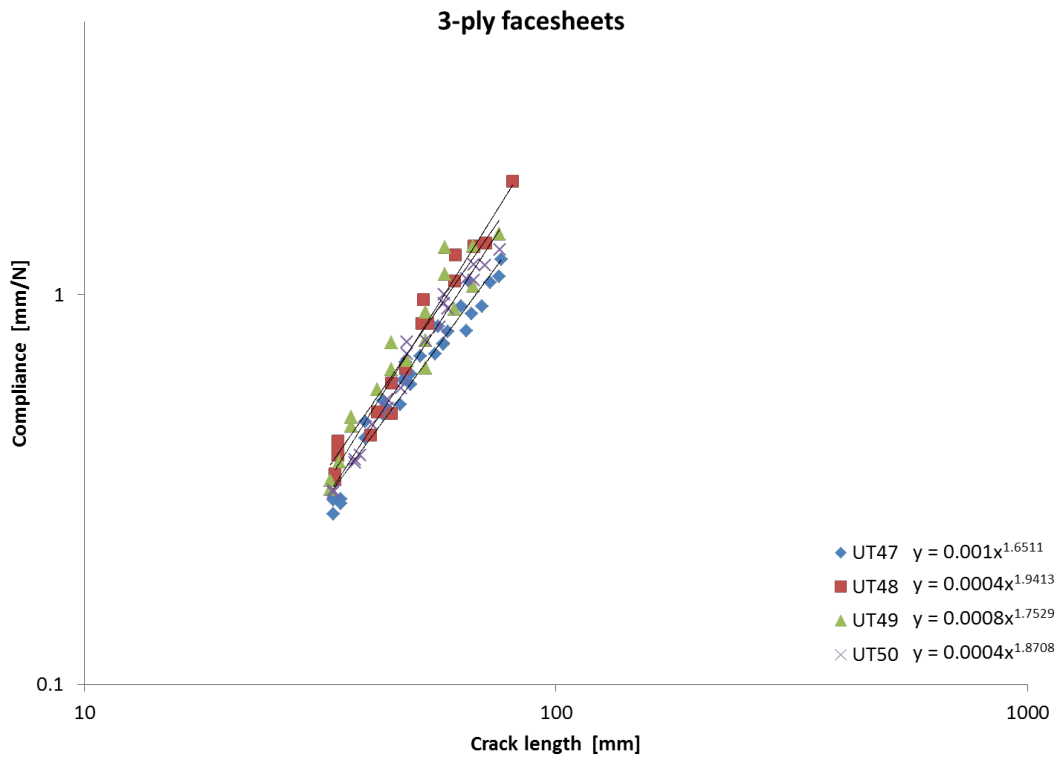


Figure 37: Compliance calibration curves in log-log scale of the SCB specimens with 3-ply facesheets.

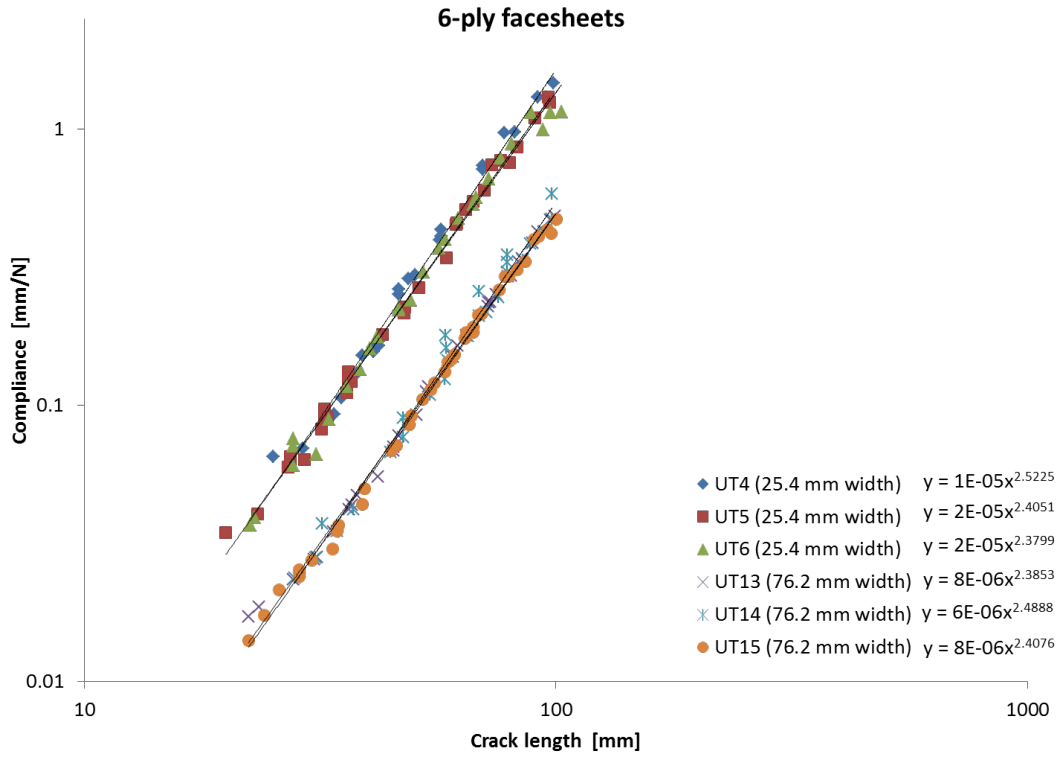


Figure 38: Compliance calibration curves in log-log scale of the 25.4 and 76.2 mm wide SCB specimens with 6-ply facesheets.

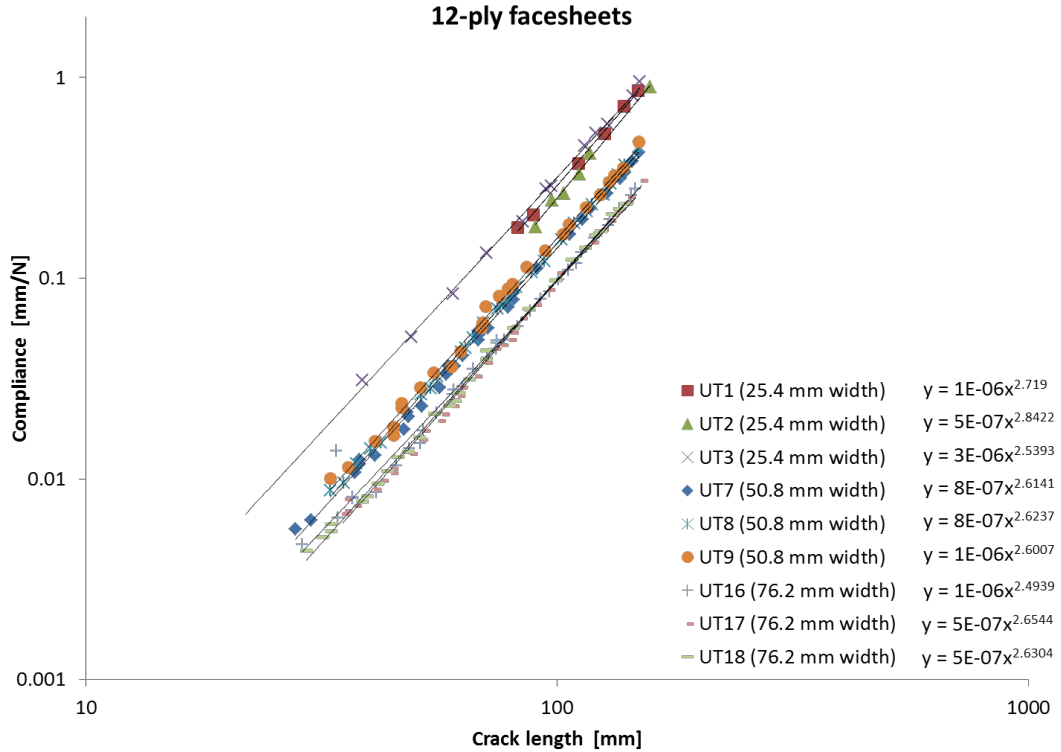


Figure 39: Compliance calibration curves in log-log scale of the 25.4, 50.8 and 76.2 mm wide SCB specimens with 12-ply facesheets.

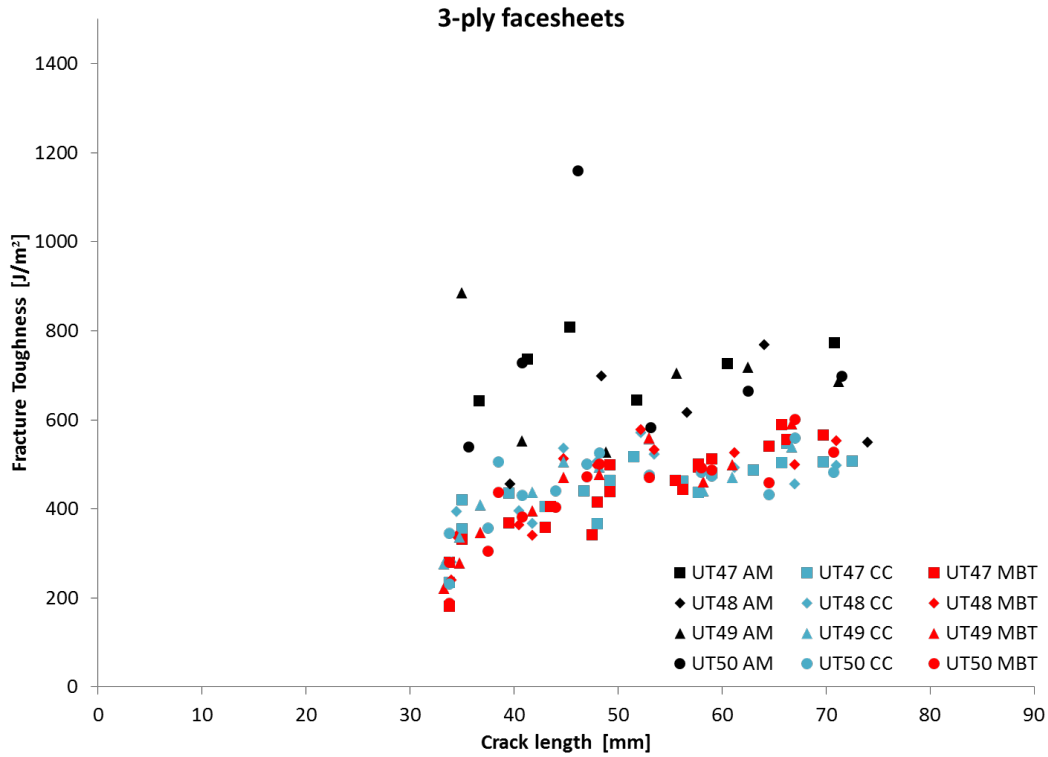


Figure 40: Apparent fracture toughness of the SCB specimens with 3-ply facesheets.

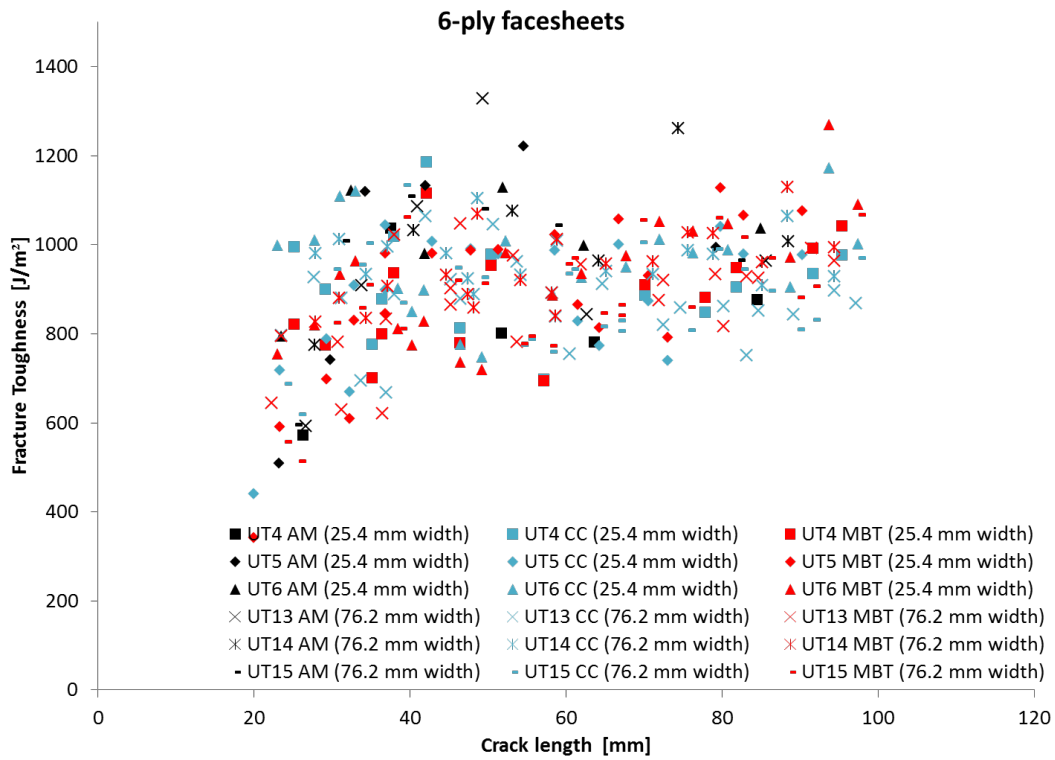


Figure 41: Apparent fracture toughness of the 25.4 and 76.2 mm wide SCB specimens with 6-ply facesheets.

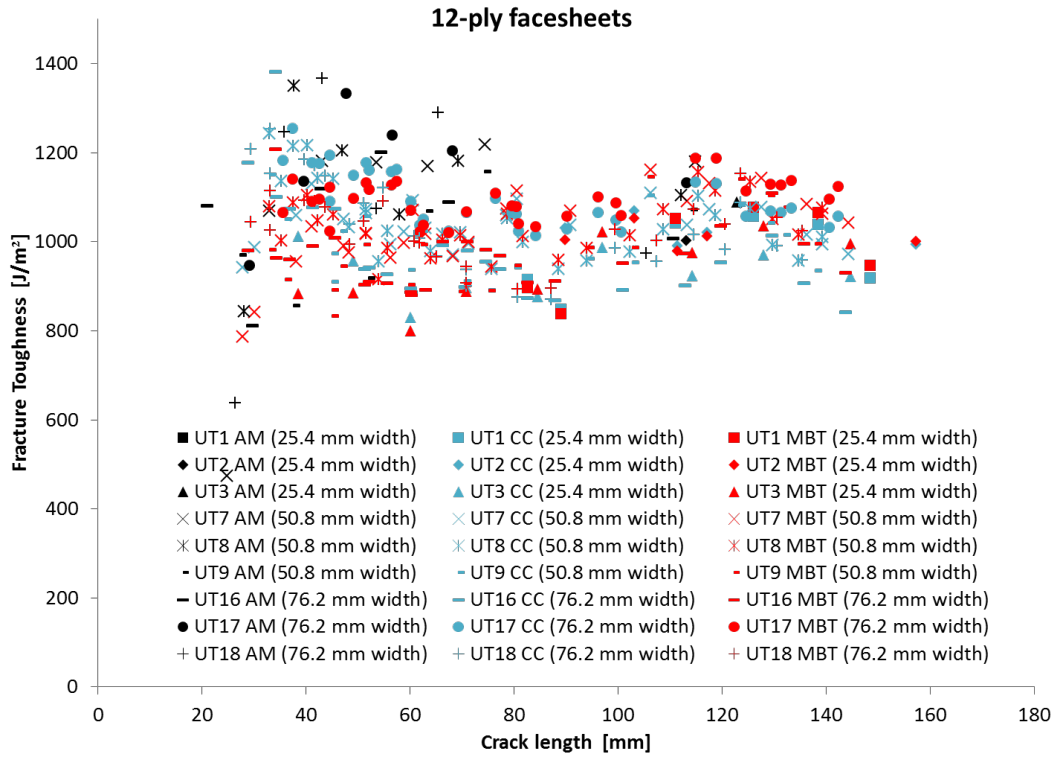


Figure 42: Apparent fracture toughness of the 25.4, 50.8 and 76.2 mm wide SCB specimens with 12-ply facesheets.

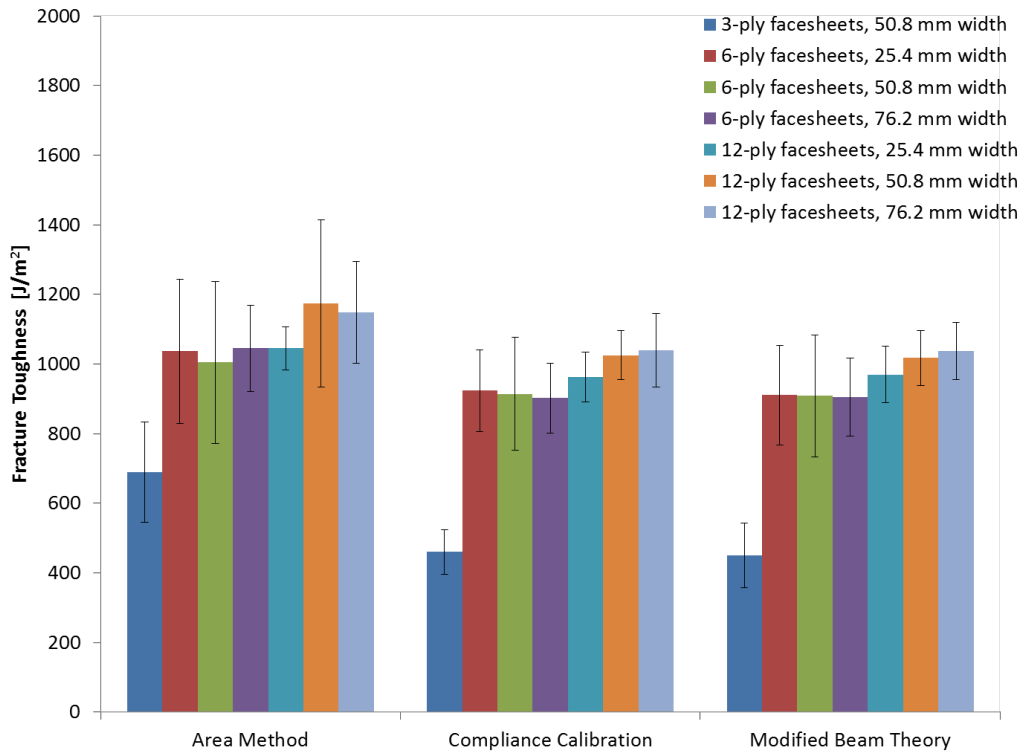


Figure 43: Apparent fracture toughness average of the SCB specimens with different facesheets and width.

REPORT DOCUMENTATION PAGE

*Form Approved
OMB No. 0704-0188*

The public reporting burden for this collection of information is estimated to average 1 hour per response, including the time for reviewing instructions, searching existing data sources, gathering and maintaining the data needed, and completing and reviewing the collection of information. Send comments regarding this burden estimate or any other aspect of this collection of information, including suggestions for reducing this burden, to Department of Defense, Washington Headquarters Services, Directorate for Information Operations and Reports (0704-0188), 1215 Jefferson Davis Highway, Suite 1204, Arlington, VA 22202-4302. Respondents should be aware that notwithstanding any other provision of law, no person shall be subject to any penalty for failing to comply with a collection of information if it does not display a currently valid OMB control number.
PLEASE DO NOT RETURN YOUR FORM TO THE ABOVE ADDRESS.

1. REPORT DATE (DD-MM-YYYY) 01-02 - 2013		2. REPORT TYPE Contractor Report		3. DATES COVERED (From - To)	
4. TITLE AND SUBTITLE Characterizing Facesheet/Core Disbonding in Honeycomb Core Sandwich Structure				5a. CONTRACT NUMBER	
				5b. GRANT NUMBER NNL09AA00A	
				5c. PROGRAM ELEMENT NUMBER	
6. AUTHOR(S) Rinker, Martin; Ratcliffe, James G.; Adams, Daniel O.; Krueger, Ronald				5d. PROJECT NUMBER	
				5e. TASK NUMBER	
				5f. WORK UNIT NUMBER 794072.02.07.03.03	
7. PERFORMING ORGANIZATION NAME(S) AND ADDRESS(ES) NASA Langley Research Center Hampton, VA 23681-2199				8. PERFORMING ORGANIZATION REPORT NUMBER NIA Report No. 2013-0015	
9. SPONSORING/MONITORING AGENCY NAME(S) AND ADDRESS(ES) National Aeronautics and Space Administration Washington, DC 20546-0001				10. SPONSOR/MONITOR'S ACRONYM(S) NASA	
				11. SPONSOR/MONITOR'S REPORT NUMBER(S) NASA/CR-2013-217959	
12. DISTRIBUTION/AVAILABILITY STATEMENT Unclassified - Unlimited Subject Category 24 Availability: NASA CASI (443) 757-5802					
13. SUPPLEMENTARY NOTES Langley Technical Monitor: Jonathan B. Ransom					
14. ABSTRACT Results are presented from an experimental investigation into facesheet core disbonding in carbon fiber reinforced plastic/Nomex honeycomb sandwich structures using a Single Cantilever Beam test. Specimens with three, six and twelve-ply facesheets were tested. Specimens with different honeycomb cores consisting of four different cell sizes were also tested, in addition to specimens with three different widths. Three different data reduction methods were employed for computing apparent fracture toughness values from the test data, namely an area method, a compliance calibration technique and a modified beam theory method. The compliance calibration and modified beam theory approaches yielded comparable apparent fracture toughness values, which were generally lower than those computed using the area method. Disbonding in the three-ply facesheet specimens took place at the facesheet/core interface and yielded the lowest apparent fracture toughness values. Disbonding in the six and twelve-ply facesheet specimens took place within the core, near to the facesheet/core interface. Specimen width was not found to have a significant effect on apparent fracture toughness. The amount of scatter in the apparent fracture toughness data was found to increase with honeycomb core cell size.					
15. SUBJECT TERMS Debonding; Facesheets; Fracture strength; Sandwich structures					
16. SECURITY CLASSIFICATION OF:			17. LIMITATION OF ABSTRACT	18. NUMBER OF PAGES	19a. NAME OF RESPONSIBLE PERSON
a. REPORT	b. ABSTRACT	c. THIS PAGE			STI Help Desk (email: help@sti.nasa.gov)
U	U	U	UU	40	19b. TELEPHONE NUMBER (Include area code) (443) 757-5802